

Cardiac-Myocyte-Specific Excision of the Vinculin Gene Disrupts Cellular Junctions, Causing Sudden Death or Dilated Cardiomyopathy[∇]

Alice E. Zemljic-Harpf,^{1,2} Joel C. Miller,^{1,2} Scott A. Henderson,³ Adam T. Wright,⁴
Ana Maria Manso,^{1,2} Laila Elsherif,^{1,2} Nancy D. Dalton,¹ Andrea K. Thor,⁵
Guy A. Perkins,⁵ Andrew D. McCulloch,⁴ and Robert S. Ross^{1,2*}

Department of Medicine, UCSD School of Medicine, La Jolla, California¹; Veterans Administration San Diego Healthcare System, San Diego, California²; Department of Physiology and the Cardiovascular Research Laboratory, UCLA School of Medicine, Los Angeles, California³; Department of Bioengineering, The Whitaker Institute for Biomedical Engineering, UCSD, La Jolla, California⁴; and National Center for Microscopy and Imaging Research Center for Research on Biological Structure, UCSD School of Medicine, San Diego, California⁵

Received 25 April 2007/Returned for modification 17 June 2007/Accepted 24 August 2007

Vinculin is a ubiquitously expressed multiliganded protein that links the actin cytoskeleton to the cell membrane. In myocytes, it is localized in protein complexes which anchor the contractile apparatus to the sarcolemma. Its function in the myocardium remains poorly understood. Therefore, we developed a mouse model with cardiac-myocyte-specific inactivation of the vinculin (Vcl) gene by using Cre-loxP technology. Sudden death was found in 49% of the knockout (cVclKO) mice younger than 3 months of age despite preservation of contractile function. Consistent telemetry documented ventricular tachycardia as the cause of sudden death, while defective myocardial conduction was detected by optical mapping. cVclKO mice that survived through the vulnerable period of sudden death developed dilated cardiomyopathy and died before 6 months of age. Prior to the onset of cardiac dysfunction, ultrastructural analysis of cVclKO heart tissue showed abnormal adherens junctions with dissolution of the intercalated disc structure, expression of the junctional proteins cadherin and β 1D integrin were reduced, and the gap junction protein connexin 43 was mislocalized to the lateral myocyte border. This is the first report of tissue-specific inactivation of the Vcl gene and shows that it is required for preservation of normal cell-cell and cell-matrix adhesive structures.

Vinculin is a 117-kDa, 1,066-amino-acid protein which is ubiquitously expressed and is a part of the complex that anchors actin to the cell membrane. It is highly conserved among diverse species, ranging from *Caenorhabditis elegans* to humans (4, 82). Sequence data and a host of biochemical and electron microscopy studies have shown that vinculin binds to a large number of proteins, including talin, paxillin, focal adhesion kinase, α -catenin, and protein kinase C- α , among others (3, 40).

The determination of vinculin's crystal structure confirmed prior data that vinculin has a head-to-tail intramolecular association (3, 10). Importantly, this interaction can mask vinculin's binding sites. One model suggested that multiple ligands need to bind vinculin for its activation (3), while others suggested that activation required binding of a single strong ligand only, such as talin or α -actinin (39). Evidence also showed that binding of acidic phospholipids, such as phosphoinositidyl-4-5-phosphate (PIP-2), to vinculin prevented its head-to-tail association (32).

With exposure of appropriate binding sites, vinculin forms a molecular bridge between the extracellular matrix and the actin-based cytoskeleton of the cell as it binds to talin, α -actinin,

paxillin, and actin. Vinculin is recruited to focal adhesions and, in doing so, may strengthen the binding of cells to extracellular matrix ligands, allowing them to resist stress from mechanical forces applied to cell surface integrins (25).

In addition to its position within the cell-matrix linkages, vinculin is also localized in the cell-cell adherens junctions that link one cell to the next (27, 28). In binding to catenins, it is recruited to the tails of cadherins and thereby detected in cellular adherens junctions (81). Recent work has shown that vinculin regulates association of β -catenin with membrane-associated guanylate-kinase inverted 2 (MAGI-2). This association leads to reduction of the tumor suppressor phosphatase and tensin homologue deleted on chromosome 10 (PTEN) by ubiquitin proteolytic degradation (70). Through this process, vinculin appears to play a critical role in the dynamic regulation of adherens junctions, at least in epithelial cells (70). Despite extensive analyses, the function of vinculin in the intact cell remains poorly understood (18, 20, 33, 63, 90).

Knowledge gained from cultured vinculin-deficient cells. Adhesion structures turn over rapidly during cell spreading and vinculin exchanges into or out of them within seconds (17). While vinculin-null embryonic fibroblasts still formed focal adhesions, these adhesions were smaller than those formed in wild-type cells and turned over more rapidly (63). Vinculin-deficient mouse F9 embryonic carcinoma cells showed alterations in cell spreading, motility, and lamellipodium formation (23). Importantly, cellular studies also

* Corresponding author. Mailing address: VA San Diego Healthcare System, 3350 La Jolla Village Drive, Cardiology Section, 111A, San Diego, CA 92161. Phone: (858) 642-1138. Fax: (858) 642-1199. E-mail: rross@ucsd.edu.

[∇] Published ahead of print on 4 September 2007.

showed that (i) cell adhesive strength can be increased exponentially by vinculin recruitment to adhesive sites, (ii) vinculin orchestrates mechanical coupling between integrins on the cell surface and the cellular cytoskeleton, and (iii) cell stiffness is reduced in the absence of vinculin (34). Work by S. W. Craig's group using Forster resonance energy transfer showed that when vinculin was recruited to the plasma membrane, its conformation changed as it was activated; ligands were bound, and therefore, the composition of proteins in the focal adhesion was altered (13). Thus, vinculin's conformation appears to correlate with functional changes in the cell membrane that occur with membrane protrusion or retraction. Fluorescent speckle microscopy of PtK1 cells was used to measure coupling between proteins in the focal adhesion and actin filaments (38) and showed that vinculin was part of the complex that provides a "molecular clutch" juxtaposed between the cytoskeleton and integrins, enabling regulation of cell migration. This compilation of work showed that vinculin stabilizes focal adhesions and that its expression level influences cell stiffness. When vinculin is expressed in its normal complement, it can protect cells from injury caused by mechanical forces.

Vinculin and cell contact sites of cardiac myocytes. As contractile cells, cardiac myocytes are basally under continuous mechanical stress. Therefore, understanding the role of vinculin in these cells is critical. Cell-cell and cell-matrix junctions in cardiac myocytes are termed intercalated discs (ICDs) and costameres, respectively. Vinculin is located in both of these locations (29, 68, 73, 75, 78). The ICDs are the most important cell-cell junction of the myocardium, joining myocytes in a staggered arrangement at their ends. Within the ICD are structures necessary for mechanical adhesion. First are fascia adherens, which dock the actin filaments to the membrane and contain proteins such as N-cadherin, catenin, and vinculin. Second are desmosomes, which link the intermediate filament desmin to the muscle termini with proteins such as desmoplakin. Both of these mechanical linkages strengthen myocytes, bridging the contractile apparatus of adjacent muscle cells. A third component of the ICD is the gap junction which is composed of connexins (Cx) and allows for rapid conductance of action potentials, thereby electrically coupling cells (16, 54).

In contrast to the ICDs at the ends of myocytes, the costamere defines the lateral cell border and is necessary for organizing myofilaments into a three-dimensional structure. Costameres were in fact first defined as "vinculin-containing bands" which encircle the myocyte perpendicular to its long axis (52). This grid-like structure organizes a series of proteins which link the sarcomere, through the cytoskeleton, to the extracellular matrix. As a multiprotein structure of organized muscle tissue, costameres are akin to the focal adhesions of cultured cells. The costamere thus also provides a site for maintenance of structure and of mechanotransduction in the contracting cardiomyocytes (62). Importantly, work by Sharp et al. (65) has shown that contractile arrest of neonatal ventricular cardiac myocytes led to depletion of vinculin from cell-matrix contact sites, while in contrast, mechanical stretch increased vinculin content. Vinculin expression was regulated in parallel with $\beta 1$ integrin. This work suggested an important

role for vinculin in maintaining the structural integrity of cardiac myocytes.

Vinculin and the intact heart. To date, few studies have explored the role of vinculin in the living organism. In humans, vinculin expression was found to be increased in the basal failing heart or in failing hearts that were not aided by a mechanical ventricular assist device (9). These data suggested that vinculin expression might increase as a means to strengthen the failing cardiac cell. In contrast, when mouse hearts were infected with *Trypanosoma cruzi*, a parasite causing Chagas' disease cardiomyopathy, vinculin expression was decreased particularly in the costameric region of myocytes, and ICD alignment was irregular, suggesting that *T. Cruzi* might in part lead to heart failure by disrupting normal vinculin expression and localization (47).

More direct data on the function of vinculin in the heart came from work on the 124-kDa splice variant isoform of vinculin termed metavinculin, which is expressed only in muscle and platelets. Metavinculin arises from a 68-amino-acid insertion at residue 915 in the vinculin sequence (7, 12, 42, 49, 69). Metavinculin appears to interact with an array of proteins within the cell similar to that observed for vinculin (8) and may account for up to 40% of the total combined pool of vinculin and metavinculin protein in vascular smooth muscle and 20 to 50% in cardiac muscle but only 6 to 8% of the total skeletal muscle pool (7). The amount of metavinculin expressed in human cardiac tissue appears greater than that in mouse (84). Metavinculin levels can be increased by mechanical loading, as has been determined with rat skeletal muscle (15). Subcellularly, metavinculin and vinculin colocalize. In vitro studies suggest that the head and tail regions of metavinculin and vinculin can interact with each other but that the rate of association of the vinculin head with the vinculin tail may be less than that of the metavinculin head with the metavinculin tail (59, 84). Studies showed that metavinculin induced an F-actin supraorganization different from that of vinculin, with fine texture F-actin filaments organized by metavinculin, compared to larger bundles with vinculin (59). These results indicate that the ratio of metavinculin to vinculin at ICDs or other cellular structures likely influences the stiffness of cells through its organization of actin. Recent reports have shown that altered expression or mutation of metavinculin can lead to cardiac dysfunction and interestingly link metavinculin abnormalities to both dilated and hypertrophic forms of human cardiomyopathy (44, 51, 76, 77).

The Vcl gene has been deleted globally the mouse. Homozygous global Vcl knockout (VclKO) mice died by embryonic day 10.5, with neural defects, aberrant forelimb development, and hearts of reduced sizes with fewer myocytes than normal. Whether the cardiac phenotype was directly caused by primary loss of vinculin expression from the cardiac myocyte or occurred due to secondary effects of vinculin protein loss from noncardiac cells led us in part to the current study. Heterozygous VclKO cells had 50% of the wild-type vinculin protein levels. Though heterozygous VclKO mice are viable and fertile and grossly do not have any abnormalities, our work has shown that they are predisposed to cardiac failure when challenged with increased hemodynamic loading (88).

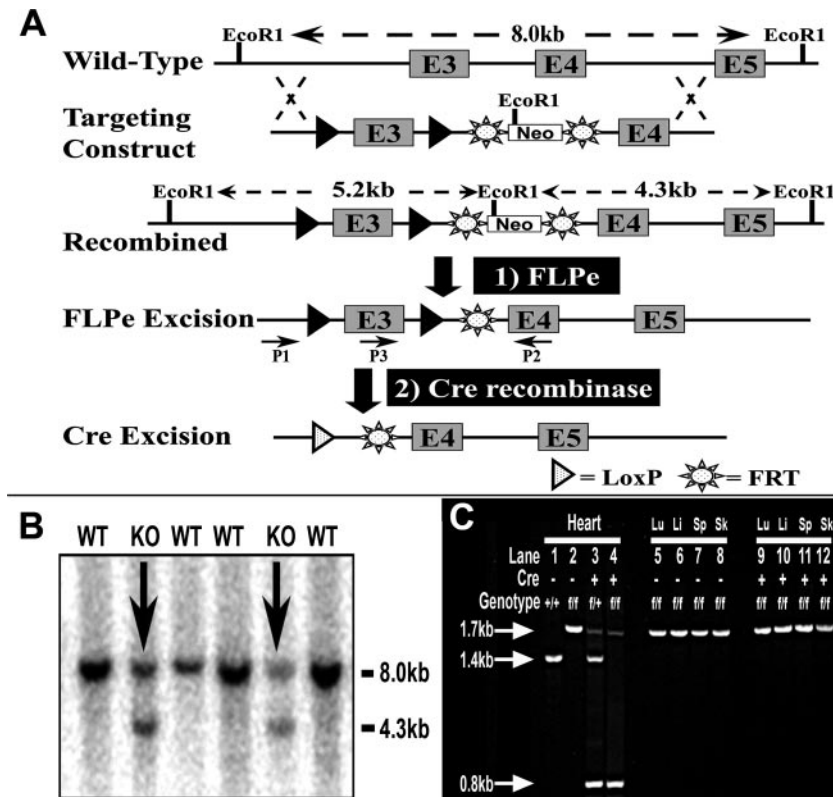


FIG. 1. Construction of floxed Vcl mice and proof of cardiac-myocyte-specific Vcl exon 3 excision. (A) Construction of “floxed” vinculin mice. In the targeting construct, *loxP* recognition sites were positioned surrounding exon 3 (E3) of the Vcl locus. A PGK-Neo resistance gene was positioned between FLP recombination target (Frt) recognition sites within intron 3. Mice with a floxed Vcl exon 3 were mated to a FLP recombinase-expressing mouse line to excise the Neo marker. Breeding to MLC2v Cre knock-in mice then directed excision of Vcl exon 3, as indicated in the lowest line of the panel. Primers utilized for genotyping as well as for assessing Cre recombinase-mediated gene excision are indicated as Pr1, Pr2, and Pr3. (B) Representative Southern blot showing ES cells which were appropriately gene targeted by the targeting construct into the Vcl locus. Genomic DNA from selected ES cells was cut with EcoRI and then screened with a labeled probe generated from the exon 5 (E5) sequence of the Vcl gene, a region located outside the targeting construct sequence. Since the Neo cassette contains a unique EcoRI site, a novel 4.3-kb band is detected in the heterozygous gene-targeted cells (KO) as distinct from the wild-type (WT) cells in which only the 8.0-kb WT allele is detected. (C) PCR was performed on DNA extracted from whole-tissue samples of heart (lanes 1 to 4) and other tissues (lung [Lu], liver [Li], spleen [Sp], and skeletal muscle [Sk]) as indicated, using primers P1 and P2 as diagrammed in panel A. A separate PCR confirmed the presence or absence of the Cre recombinase allele. A 1.4-kb band represents the WT Vcl allele, a 1.7-kb band is generated from the gene-targeted (floxed) Vcl allele, and a 0.8-kb fragment represents excision of exon 3. The 0.8-kb excision band was detected only in heart tissue from heterozygous or homozygous Vcl “floxed” mice and only when Cre recombinase was simultaneously expressed (lanes 3 and 4, Vcl^{f/+} MLC2v^{Cre/+} and Vcl^{f/f} MLC2v^{Cre/+}, respectively). This 0.8-kb fragment was not detected in any other tissue surveyed from the Vcl^{f/f} MLC2v^{Cre/+} mice, even when Cre recombinase was present (lanes 5 to 12). f, floxed allele.

We hypothesized that vinculin was critical for the mechanical stability of cardiac myocytes, since it is an actin-binding protein positioned for anchoring the sarcomere to the cell membrane as well as one myocyte to the next. For this purpose, we constructed a novel mouse model where reduction of vinculin/metavinculin occurs only in cardiac myocytes. In this report, we show that loss of vinculin from myocytes results in sudden death or heart failure. Structural, biochemical, and microscopic analyses revealed remodeling of cell-matrix and cell-cell junctions. This *in vivo* model greatly advances our understanding of vinculin’s function.

MATERIALS AND METHODS

Generation of the floxed Vcl targeting construct. PCR was used to derive fragments of the Vcl genomic sequence. For this, a 129/Sv mouse genomic clone was used as a template (86). Three fragments were used for construction: (i) a 5’

flanking fragment (2,043 bp) composed of Vcl intron 2 sequence, (ii) a middle (847-bp) fragment composed of 369 bp of intron 2, exon 3 (151 bp), and 327 bp of intron 3, and (iii) a 3’ fragment (2,182 bp) composed of 315 bp of intron 3, 109 bp of exon 4, and 1,758 bp of intron 4. The resulting construct positioned the middle (exon 3)-containing fragment between *loxP* recognition sites and a phosphoglycerate kinase (PGK)-neomycin (Neo) selection cassette between FLP recombination target recognition sites (Fig. 1A). The targeting vector sequence was confirmed, and then 129/Sv-LW1 embryonic stem (ES) cells were electroporated with the linearized targeting vector. Neo-resistant clones were characterized further as described below.

Genotyping of cVclKO mice. The genotypes of the mice were determined by PCR as shown in Fig. 1A. Primers P3 (5’-CCTGCGCGGGATTACCTCATTGAC-3’) and P2 (5’-TGCTCACTGGCCCAAGATTCTTT-3’) allowed detection of the recombinant allele, producing an 843-bp band from the wild-type allele and a 960-bp band from the floxed allele. To assess for Cre recombinase expression, primers CreF (5’-GTTCGCAAGAACCTGATGCACA-3’) and CreR (5’-CTAGAGCCTGTTTTGCACGTTTC-3’) were used to produce a 350-bp Cre product. PCR conditions were 1 cycle of 1 min at 94°C, 35 cycles of 30 s at 58°C, 1 cycle of 30 s at 72°C, and 1 cycle of 10 min at 72°C. Cre-mediated excision of

Vcl exon 3 was confirmed by PCR analysis using primers P1 (5'-TTACGCCTA GCCTTGAA-3') and P2 (described above) (Fig. 1A) with the following conditions: 1 cycle of 30 s at 94°C, 35 cycles of 30 s at 54°C, 1 cycle of 30 s at 72°C, and 1 cycle of 10 min at 72°C. All animal study protocols were approved by the institutional review committee, and all mice were housed in an AAALAC-approved facility.

Antibodies and fluorochromes. The following antibodies were used: mouse monoclonal anti-pan-vinculin (which detects both vinculin and metavinculin) (clone hVin-1, V9131; Sigma, St. Louis, MO); rabbit polyclonal anti-pan cadherin (C3678; Sigma), rabbit polyclonal anti-connexin 43 (anti-Cx43, C6219; Sigma), rabbit polyclonal anti- β 1D integrin (55), rabbit polyclonal anti-desmoplakin (AHP 320; Serotec, Raleigh, NC), rabbit polyclonal anti-dystrophin (E2664; Spring Bioscience, Fremont, CA), mouse monoclonal anti-glyceraldehyde-3-phosphate dehydrogenase (GAPDH) (TRK5G4-6C5; RDI Division of Fitzgerald Industries International, Concord, MA), horseradish peroxidase-conjugated anti mouse/anti-rabbit (115-175-146/771-035-152; Jackson ImmunoResearch, West Grove, PA), Alexa Fluor 488 goat anti-mouse (A-11029; Molecular Probes, Invitrogen, Carlsbad, CA), and Alexa Fluor 568 goat anti-rabbit (Molecular Probes, Invitrogen, A-11036).

Western blotting. Freshly isolated hearts were immediately frozen in liquid nitrogen, pulverized, homogenized in modified radioimmunoprecipitation assay buffer, and analyzed via techniques described previously (2, 64). Whole-heart protein lysate was resolved by sodium dodecyl sulfate-polyacrylamide gel electrophoresis, and Western blots were performed to detect vinculin/metavinculin and GAPDH. Blots were incubated with primary antibodies overnight at 4°C. Dilutions were anti-vinculin (1:5,000) and anti-GAPDH (1:5,000 to 1:30,000). Densitometric quantitation of protein bands was performed digitally (ChemImager 4400; Alpha Innotech Corp., San Leandro, CA).

Quantitative real-time RT-PCR. For real-time PCR studies, total RNA was isolated from hearts of 9- to 12-week-old male mice by using RNA-Bee (Tel-Test, Inc., Friendswood, TX) according to the manufacturer's protocols. Real-time reverse transcriptase PCR (RT-PCR) was carried out using a QuantiTect SYBR green RT-PCR Kit (QIAGEN, Valencia, CA), following the manufacturer's protocol. Thirty nanograms of RNA was used as a template. The primers used for quantitation were as follows: ANF-1 (5'-CATCACCTGGGCTTCTT CCT-3'), ANF-2 (5'-TGGGCTCCAATCCTGTCAATC-3'), BNP-1 (5'-GCGG CATGGATCTCCTGAAGG-3'), BNP-2 (5'-CCCAGGCAGAGTCAGAACT G-3'), GAPDH-1 (5'-ATGTTCCAGTATGACTCCTCACTCAG-3'), GAPDH-2 (5'-GAAGACACCAGTAGACTCCACGACA-3'), Metavinculin-1 (5'-CTTTC CCCTTGACATGGAA-3'), and Metavinculin-2 (5'-GAATAAGTGCCCGCT TGGTA-3').

The PCR conditions were 30 min at 50°C and 15 min at 95°C for reverse transcription and then 44 cycles of 30 s at 94°C, 30 s at 56°C, and 40 s at 72°C for all primer sets except metavinculin, which used 40 cycles of 15 s at 95°C, 60 s at 62°C, and 40 s at 72°C. All reactions were performed using a PCR real-time thermocycler (model 7300; Applied Biosystems, Foster City, CA).

Tissue acquisition, morphometry, histology, electron microscopy, and immunofluorescence microscopy. For morphometric analyses, the animals were sacrificed at the ages indicated in the text. At sacrifice, hearts were arrested in diastole by injection of a high-potassium solution (25 mM KCl and 5% dextrose in 1× phosphate-buffered saline). Heart tissue was preserved, and immunofluorescence was performed as previously described (64). Ten-micrometer cryosections were prepared via standard techniques and stained with antibodies as outlined previously (2). Antibodies were diluted as follows: anti-vinculin, 1:700; anti-pan cadherin, 1:600; anti-connexin-43, 1:600; anti-desmoplakin, 1:600; anti- β 1D integrin, 1:1,500; anti-dystrophin, 1:100; and all secondary antibodies, 1:300. Control sections stained with the primary antibodies alone did not detect autofluorescence of the heart tissue, and no significant background fluorescence was evident in the sections stained with secondary antibody alone. The results were visualized via a confocal microscope (Zeiss LSM 510) or one with deconvolution optics (DeltaVision software; Applied Precision, Inc., Seattle, WA).

For transmission electron microscopy studies, five samples from each genotype were analyzed. The samples were fixed in Karnovsky's fixative (4% paraformaldehyde, 2.5% glutaraldehyde, 5 mM CaCl₂ in 0.1 M Na cacodylate buffer, pH 7.4) overnight at 4°C, followed by treatment with 1% OsO₄ in 0.1 M Na cacodylate buffer, pH 7.4, for 1 h at room temperature. Tissue pieces were then en bloc stained with 4% uranyl acetate in 50% ethanol and subsequently dehydrated using a graded series of ethanol solutions, followed by treatment with propylene oxide and infiltration with epoxy resin (Scipoxy 812; Energy Beam Sciences, Agawam, MA). After polymerization at 65°C overnight, ultrathin sections (70 to 80 nm) were stained with lead citrate, and electron micrographs were recorded by using an electron microscope (1200EX; JEOL) operated at 80 kV (88).

Physiological, surgical, and echocardiographic procedures. Invasive hemodynamic determinations were performed at baseline, following dobutamine infusions, as previously described (64, 88). Briefly, animals were anesthetized via intraperitoneal injection of 100 mg/kg ketamine and 5 mg/kg xylazine and placed on a warming pad. Heart rate and temperature were continuously monitored. Following anesthetization and intubation, both vagus nerves were cut and the right carotid artery was exposed. A 1.4 French micromanometer-tipped catheter (Millar Instruments, Houston, TX) was inserted and advanced until a left ventricular pressure tracing was visualized. The catheter was adjusted so that no catheter trapping was evident. The animals were recovered from the initial procedure, and baseline pressure measurements were obtained. Sequential, continuous perfusions of graded dobutamine doses (1, 2, 4, and 8 mg/kg/min) were administered for 3 minutes at each dose. The measurements were acquired, digitized, displayed, and analyzed with the Datasciences/Ponemah Physiology Platform program (V4.40; Datasciences/Ponemah, St. Paul, MN). All hemodynamic data were recorded continuously to ensure stable levels of pressures and heart rates. Data from the last 30 seconds of each dose interval were used for analysis.

Conscious telemetry utilizing an implantable wireless transmitter/receiver system (Datasciences/Ponemah) was performed on mice. For all implantation procedures, the mice were anesthetized with ketamine (100 mg/kg)-xylazine (5 mg/kg) and monitored continuously. Under the stereomicroscope, incisions were made along the abdominal midline caudal to the xyphoid process, right axillary and horizontally, along the left fifth intercostal space. A radio transmitter (ETA-F20; Datasciences) was inserted into the abdominal cavity and secured via sutures to the parietal peritoneum and muscular fascia. Two leads were tunneled through the subcutaneous space to reach the thoracic wall overlying the apex of the heart and the right acromion and were sutured in place. The incisions were closed in layers, and the animal was allowed to recover. For monitoring, animals were housed singly in Plexiglas cages and fed food and water ad libitum. A 24-h diurnal light cycle was maintained, with standard 12-h-on and 12-h-off cycles (0700 to 1900 on, 1900 to 0700 off). Transmitters were detected by receiver platforms placed directly underneath the animal's cage. The receiver platforms were linked to an immediately adjacent computer. Dataquest ART 2.0 data acquisition software (Datasciences) was used for digitization of the signal (at a sampling rate of 1,000 Hz) and for on-line display of the electrocardiogram as well as for data storage onto a hard disk. Studies were recorded continuously beginning 72 h following recovery from the implantation.

Echocardiography (M-mode, two-dimensional, and Doppler) was performed on animals under isoflurane anesthesia and measured by investigators blinded to the genotype of the animal, as previously described (88).

Optical mapping. Optical studies were performed on isolated murine hearts from 8-week-old mice ($n = 7$ for each group [cVclKO and control]) with the potentiometric dye Di-4-ANEPPS, and the left ventricular epicardium was optically mapped with a high-speed charge-coupled-device camera. Motion artifact was attenuated with perfusion of 15 mM 2,3-butanedione monoxime. Epicardial-action-potential propagation was mapped during intrinsic rhythm and ventricular pacing. In these studies, 5 seconds of data per run was acquired, with views of the epicardium mapped at 64-by-64 pixel images in 12-bit format, using a high-speed camera at 950 frames/second. Spatial phase shift and temporal median filtering were implemented, and activation at each pixel was identified at the maximum rate of change of fluorescence, as described previously (71). During ventricular pacing, local curvature was quantified by calculating the gradient of the normalized conduction velocity vector field (6). A disorganized wave front can be quantified by a greater negative curvature (37), indicating areas of local conduction delay or heterogeneity.

Statistical methods. Data were compiled and are shown as means \pm standard errors of the means. Unless noted, data were evaluated using unpaired, two-tailed t tests (95% confidence interval) or two-way repeated-measure analyses of variance with post hoc analysis using a Bonferroni test and GraphPad Prism4 software (GraphPad Inc, San Diego, CA). Genotypic analysis for comparing observed versus expected frequencies was evaluated using Chisquare analysis. A P value of <0.05 was considered significant.

RESULTS

Mice with a floxed Vcl allele have been created to allow tissue-specific gene excision. We adapted the successful gene targeting strategy from global VclKO mice to allow for tissue-specific gene excision at the Vcl locus. A diagram of the wild-type and recombined alleles is shown in Fig. 1A. Targeting

exon 3 of the *Vcl* gene provided a strategy which resulted in reduction of both vinculin and metavinculin protein expression as shown previously (86, 88). This occurs since exon 3 consists of 51 nucleotides and when deleted causes alteration in the open reading frame of the *Vcl* gene, with generation of a premature stop codon at nucleotide 385 of the mutant transcript. Metavinculin is coded for by exon 19 of the *Vcl* gene; thus, it is located far downstream of the targeted exon and premature stop. Appropriate homologous recombination of the “floxed” targeting construct into the *Vcl* locus was detected by Southern blotting of EcoRI-cut genomic DNA with both a 5′ probe internal to the targeting vector (*Vcl* exon 3 sequence) and a 3′ probe external to the targeting vector (composed of *Vcl* exon 5 sequence). An EcoRI restriction site found in the Neo cassette allowed generation of unique restriction fragments in the targeted allele. Successfully targeted clones yielded a 5.2-kb fragment with the 5′ probe and a 4.3-kb fragment with the 3′ (exon 5) probe, in contrast to the 8.0-kb fragment detected by both probes on wild-type genomic DNA (Fig. 1B). Clones judged to be successfully targeted were further confirmed by PCR and then used for microinjection into C57BL/6 mouse blastocysts. Mice with successful germ line transmission of the targeted allele were identified and termed *Vcl* “floxed” mice. The heterozygous *Vcl* “floxed” mice (*Vcl*^{fl/+}) still contained the selectable marker cassette PGK-Neo and thus were mated to FlpE recombinase deleter mice (58) [Tg(CTFLPe)9205Dym; Jackson Laboratories, Bar Harbor, ME] to excise the selectable marker (Fig. 1A). PCR was used to confirm appropriate FlpE-mediated excision of the Neo selectable marker (data not shown). Subsequently, the mice were bred with a mouse line which expresses ventricular myosin light chain-2 (*MLC2v*)-Cre recombinase via a knock-in allele (14) (Fig. 1A). These mice express Cre recombinase only in ventricular cardiac myocytes and cause gene excision and protein reduction beginning in the perinatal period (19, 53, 64). Homozygous floxed *Vcl* mice (*Vcl*^{fl/fl}) that also expressed the cardiac-myocyte-specific Cre recombinase (*Vcl*^{fl/fl} *MLC2v*^{Cre/+}) were termed cVclKO. Cre-negative littermates with the genotype *Vcl*^{fl/fl} *MLC2v*^{+/+} were used and termed “control” mice. All mice were bred and maintained in a mixed genetic background (SV129/Black Swiss).

To assess for Cre-mediated gene excision, DNA was prepared from whole tissues as indicated and PCR was used with primers 5′ and 3′ of *Vcl* exon 3, termed primers P1 and P2 (Fig. 1A). PCR with this primer set produced a 1.4-kb product for the wild-type exon 3 allele, a 1.7-kb product for the unexcised, floxed exon 3 allele, and an 0.8-kb amplicon only following Cre-mediated excision of the *Vcl* allele (Fig. 1C). The 0.8-kb band was detected only in heart samples from mice that also expressed Cre-recombinase (Fig. 1C, lanes 3 and 4), not in heart samples from mice that did not express Cre (Fig. 1C, lanes 1 and 2) or from any other tissue, whether Cre expression was present or not (Fig. 1C, lanes 5 to 12). The 1.7-kb product was still detected in whole-heart DNA samples, even when Cre recombinase was expressed (Fig. 1C, lanes 3 and 4), since Cre-mediated excision did not occur in all myocytes, and also since DNA from nonmyocytes was still present in this sample. Thus, mice in which the *Vcl* gene could be excised specifically in cardiac myocytes were created.

TABLE 1. Genotypes of offspring from a breeding scheme which used parental strains *Vcl*^{fl/fl} *MLC2v*^{Cre/+} and *Vcl*^{fl/fl} *MLC2v*^{+/+}

Mouse group ^b	No. (%) of mice of indicated sex		Total no. (%) of mice	
	Male	Female	Observed	Expected
<i>Vcl</i> ^{fl/fl} <i>MLC2v</i> ^{Cre/+} (cVclKO)	107 (24.3)	97 (22.1)	204 (46)	220 (50)
<i>Vcl</i> ^{fl/fl} <i>MLC2v</i> ^{+/+} (control)	125 (28.4)	111 (25.2)	236 (54)	220 (50)
Total	232	208	440	440

^a Crosses of these parental-strain mice produced progeny with genotypes *Vcl*^{fl/fl} *MLC2v*^{Cre/+} and *Vcl*^{fl/fl} *MLC2v*^{+/+} with expected ratios of 1:1 when all offspring were viable. Offspring were observed to show appropriate Mendelian ratios. (The chi-square value was 2.327 with 1 degree of freedom. The two-tailed *P* value was 0.127 between the observed and expected genotypes.)

^b Fifty-six litters (440 mice).

Cardiac-myocyte vinculin deficiency leads to high mortality rates. Genotypic analysis of mice at weaning age detected animals homozygous for the floxed vinculin allele that were also positive for the *MLC2v*-Cre allele. Initial evaluation showed that these mice could survive to adulthood. Therefore, *Vcl*^{fl/fl} *MLC2v*^{Cre/+} mice were bred with *Vcl*^{fl/fl} *MLC2v*^{+/+} mice. Evaluation of 56 litters from such a breeding scheme resulted in 440 live births. The genotypes of these mice as shown in Table 1 indicated that the cVclKO mice survived to a weaning age (3 weeks of age) and had expected Mendelian ratios. To assess *Vcl* gene expression in our cVclKO model, we compared the relative vinculin/metavinculin protein contents in the control and cVclKO hearts. Since vinculin is expressed in myocytes and nonmyocyte cells in the heart (74) and *MLC2v*-Cre is expressed only in the ventricular myocytes, the best way to make this comparison is to use protein lysates from isolates of ventricular myocytes of the adult mouse myocardium. To isolate adult ventricular myocytes, we routinely perform collagenase digestion of the heart via retrograde perfusion of the aorta (Langendorff retrograde perfusion) (50). Healthy, rod-shaped myocytes could be easily isolated in high numbers from wild-type mice as well as control mice. In contrast, hearts from the cVclKO mice gave reproducibly low yields of rod-shaped myocytes, with very poor plating efficiency, even when collagenase concentration was varied and/or digestion time was reduced, indicating that vinculin-null cardiac myocytes were fragile and intolerant to isolation. Given these results, we turned to alternative methods to assess how expression of vinculin/metavinculin had changed in the cVclKO hearts. Since metavinculin is expressed only in muscle cells within the myocardium (7, 8), we assessed how the metavinculin transcript was altered using real-time PCR and how its protein expression changed via Western blotting of samples from intact cVclKO hearts compared to those from control littermates (Fig. 2A and B). Three-month-old cVclKO mice showed a 57% reduction of metavinculin transcript expression, normalized to GAPDH transcript levels (Fig. 2A) ($n = 4$ for each group, $P < 0.009$ for comparison with controls), and a 71% reduction of metavinculin protein expression (Fig. 2B) compared to what was found for littermate control animals. Densitometric analysis was performed

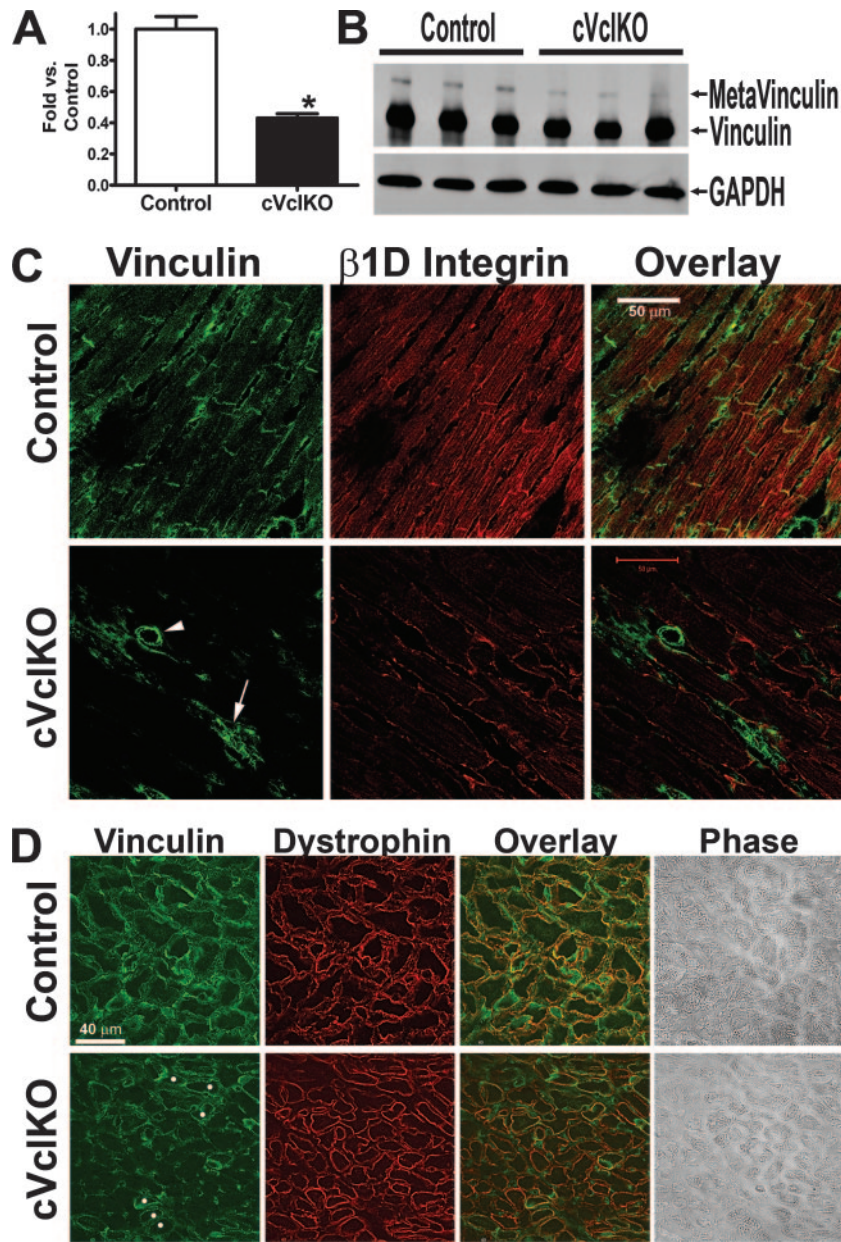


FIG. 2. The expression of metavinculin transcript and protein is significantly reduced in heart, and vinculin/metavinculin immunoreactive expression is reduced in cardiac myocytes. (A and B) Whole-heart samples from 12-week-old mice were analyzed by using either real-time RT-PCR (A) or Western blotting (B). Since metavinculin is expressed only in cardiac myocytes within heart, its reduction was used to assess reduction of the total vinculin/metavinculin pool, which would be reduced in the myocytes. In each case, evaluation was made so that metavinculin expression was normalized to GAPDH expression. cVclKO hearts showed a 57% reduction of normalized metavinculin transcript expression compared to control hearts (A) ($n = 4$ for each group; *, $P < 0.009$), while a 71% reduction of metavinculin protein expression was found in cVclKO hearts compared to littermate control levels (B) ($n = 6$ for each group; $P < 0.0007$ for densitometric data from Western blotting; data not shown). Vinculin protein expression was still detected since it was present in nonmyocytes as well as a portion of myocytes. (C and D) Microscopic analysis of myocardial tissue showed that vinculin is absent in a large number of cardiac myocytes from cVclKO mice. Immunostaining using an anti-muscle specific $\beta 1D$ integrin antibody (C) or an anti-dystrophin antibody (D) was used to specifically visualize myocytes in longitudinal orientation (C) or in a cross-section (D). Vinculin was still expressed in cells of blood vessels (arrowhead in panel C), nonmyocytes (arrow in panel C), and a portion of myocytes (white dots in panel D) in cVclKO hearts.

by normalizing metavinculin expression to simultaneously measured GAPDH expression ($n = 6$ for each group for Western blotting, $P < 0.0007$ for comparison with controls) (data not shown). Residual vinculin expression was detected in the cVclKO samples since they were from whole heart,

and vinculin was still expressed at normal levels in the non-myocyte component and a small percentage of myocytes within these lysates. Microscopic evaluation of cardiac tissue from cVclKO and control tissue was performed using an anti-vinculin antibody which detected both vinculin and

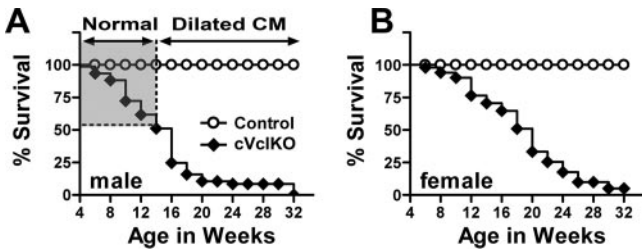


FIG. 3. Cardiac-myocyte-specific excision of the vinculin gene causes high mortality rates in cVclKO mice. (A) Male survival curves. (B) Female survival curves. Gender affects the mortality rate in cVclKO mice. By 14 weeks of age, only 51% of male cVclKO mice survived (A) (cVclKO $n = 49$, control $n = 37$), compared to 71% survival of cVclKO female mice (B) (cVclKO $n = 66$, control $n = 52$). Male mice older than 14 weeks developed dilated cardiomyopathy (CM) and showed a more rapid mortality than female mice. No male mice survived past 32 weeks of age compared to 4% of female cVclKO surviving until this age. The gray box in panel A denotes the age range during which mice were found to die suddenly but still had normal cardiac systolic function.

metavinculin expression in all cells and two antibodies which would detect expression of protein in muscle only (an anti- β 1D integrin isoform-specific antibody which detected integrin expression only in myocytes, since the D isoform of this integrin has muscle-restricted expression (55) (Fig. 2C) or dystrophin [Fig. 2D]). In cVclKO hearts, vinculin/metavinculin-null myocytes were clearly visualized, but residual vinculin expression was detected in vessels, nonmyocytes, and patches of myocytes, in agreement with previous studies which also used MLC2v-Cre for excision of floxed genes (64).

Initially, cVclKO mice were visibly indistinguishable from their littermate controls. Despite appearing healthy, many of the cVclKO mice were observed to die suddenly. Therefore, we followed the cVclKO mice as well as matched controls on a daily basis for 6 months as shown in Figure 3A and B (for cVclKO mice, male $n = 66$, female $n = 49$).

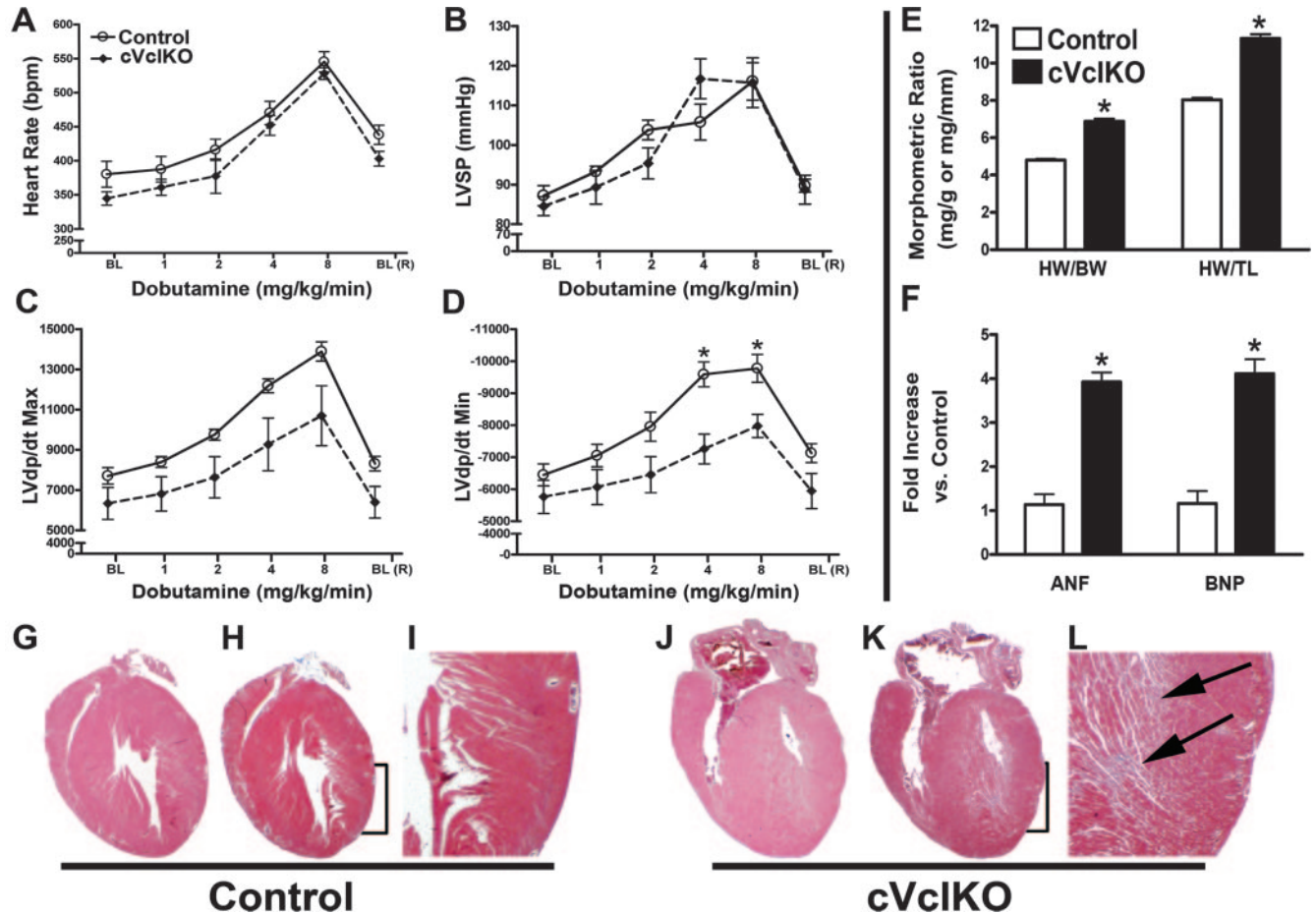


FIG. 4. Young cVclKO mice show cardiac hypertrophy with preserved systolic function and mild diastolic dysfunction. (A to D) Millar catheterization of 9- to 14-week-old male cVclKO and control mice showed no differences in basal or dobutamine-stimulated heart rate (A), left ventricular systolic pressure (LVSP) (B), or LV dp/dt_{max} (C), or LV dp/dt_{min} (D) was significantly reduced in cVclKO mice compared to that in control mice (cVclKO $n = 6$, control $n = 5$; *, $P < 0.004$ for 4 mg/kg/min and $P < 0.01$ for 8 mg/kg/min). BL, baseline; BL (R), return to baseline. (E and F) Morphometry and molecular markers show that 8- to 11-week-old cVclKO mice develop cardiac hypertrophy. (E) Increased heart weight/body weight (HW/BW) and heart weight/tibia length (HW/TL) ratios were seen in cVclKO mice compared to those in control mice (*, $P < 0.006$ for HW/BW and $P < 0.003$ for HW/TL; cVclKO $n = 24$, control $n = 19$). (F) The hypertrophic markers ANF and BNP were quantified by real-time RT-PCR and were upregulated in cVclKO mice compared to those in control mice (for ANF, 3.9-fold [*], $P < 0.007$), and for BNP, 4.1-fold [*], $P < 0.02$; $n = 5$). (G to L) Histological analysis of myocardial tissue of 10-week-old control (G to I) and cVclKO (J to L) mice stained with hematoxylin and eosin (G and J) as well as trichrome (H, I, K, and L) showed right and left ventricular hypertrophy but only mild fibrosis (arrows in panel L) in cVclKO hearts compared to what was found for littermate controls. (Panels I and L are magnified views from the bracketed regions of panels H and K, respectively.)

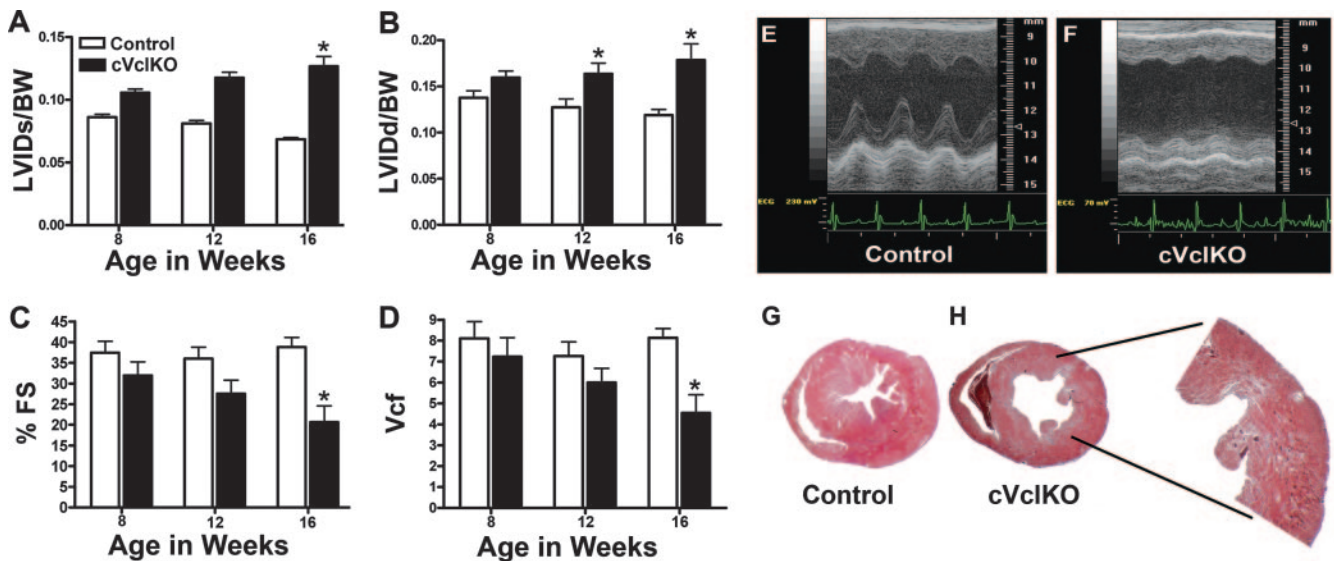


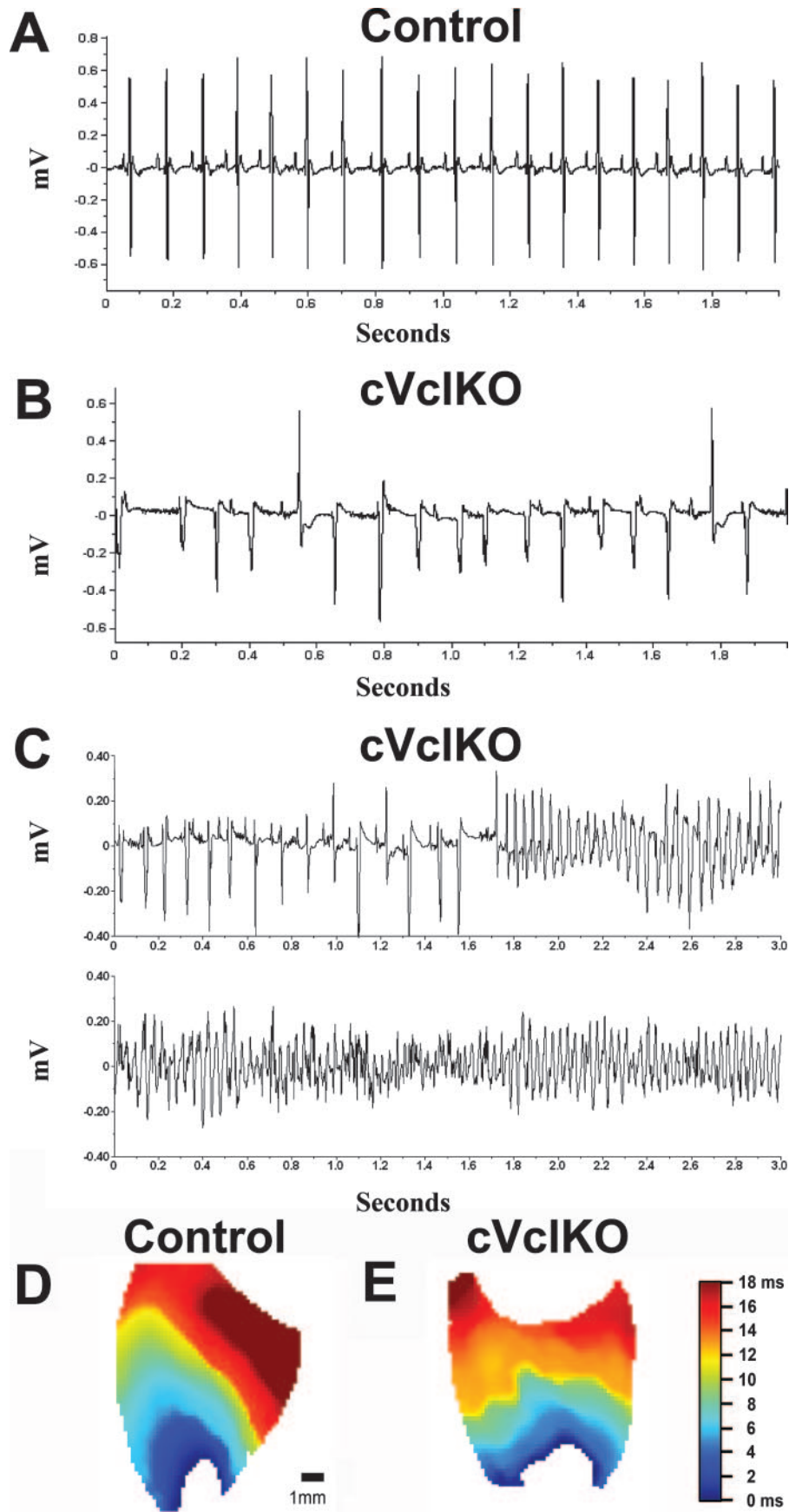
FIG. 5. Hearts of 16-week-old cVclKO mice show dilated cardiomyopathy and cardiac fibrosis. (A to F) Echocardiographic data. Animals were evaluated by echocardiography under basal conditions at 8, 12, and 16 weeks of age. Heart function was similar in 8- and 12-week-old cVclKO and control mice, but by 16 weeks, the cVclKO mice showed left ventricular dilation as well as impaired cardiac function (at 8 weeks, control $n = 8$, cVclKO $n = 11$; at 12 weeks, control $n = 8$, cVclKO $n = 11$; at 16 weeks, control $n = 8$, cVclKO $n = 5$). (A and B) Indexed left ventricular dimensions of control and cVclKO mice in systole (A) (*, $P < 0.002$ for cVclKO versus control levels at 16 weeks) and diastole (B) (*, $P < 0.03$ for cVclKO versus control levels at 12 weeks and $P < 0.002$ for cVclKO versus control levels at 16 weeks). (C and D) Ventricular function as indicated by %FS (C) and Vcf (D) (*, $P < 0.001$ for cVclKO versus control levels at 16 weeks for both %FS and Vcf). (E and F) M-mode echocardiograms from 16-week-old control (E) and cVclKO (F) mice. LVIDs/BW, left ventricular internal dimension in systole with respect to body weight; LVIDd/BW, left ventricular internal dimension in diastole with respect to body weight. %FS refers to left ventricular fractional shortening. (G to H) Histological analysis of myocardial tissue from 16-week-old control (G) and cVclKO (H) hearts stained with trichrome showed left ventricular dilation and replacement fibrosis in right and left ventricles of cVclKO mice compared to what was found for littermate controls.

Beginning at 6 weeks of age, male mice displayed a more rapid mortality than female mice (Fig. 3A and B). Young cVclKO mice that died suddenly did not show any signs or postmortem evidence of cardiomyopathy (Fig. 3A, gray outlined area). In contrast, male and female mice older than 14 weeks of age showed clear signs, symptoms, and postmortem evidence of heart failure. Given the more accelerated findings in male cVclKO mice, this gender was utilized for the subsequent studies.

Young adult male cVclKO mice have normal systolic cardiac function, with molecular and morphological evidence of cardiac hypertrophy. Next, we evaluated cVclKO mice at discrete time points. First, cardiac function was assessed in 9- to 12-week-old mice by invasive catheterization with a micromanometer-tipped catheter. No differences in heart rate, systemic blood pressure, or contractility (maximum rate of pressure increase with respect to time [LV dP/dt_{max}]) were evident between cVclKO and control mice (Fig. 4A to C). Relaxation as estimated by LV dP/dt_{min} was normal in the cVclKO mice at baseline and with several doses of dobutamine, but abnormalities at the higher dobutamine doses were found, consistent with mild diastolic dysfunction (Fig. 4D). Morphometric ratios (heart weight/body weight and heart weight/tibia length) as well as atrial natriuretic factor and brain natriuretic peptide transcript levels were increased in the cVclKO mice at this age, consistent with evidence of mild morphometric and molecular cardiac hypertrophy (Fig. 4E and F). Histological evaluation showed

that cVclKO hearts had morphological hypertrophy and only mild fibrosis (Fig. 4G to J). Despite these findings, by 14 weeks of age, 49% of male cVclKO mice died suddenly. Mortality in these younger age cVclKO mice was therefore not due to systolic failure.

cVclKO mice which survive sudden death later develop a dilated cardiomyopathy. Since the survival rates of the cVclKO mice continued to decline as they aged (Fig. 3A, Dilated CM), we followed the function of the mice with successive echocardiograms. As shown in Fig. 5A to F, there was progressive dilation of the left ventricle in systole and diastole (Fig. 5A and B) which paralleled the decline in overall ventricular function, evidenced by reduction of percent fractional shortening (%FS) and velocity of circumferential fiber shortening (Vcf) (Fig. 5C and D). These findings are consistent with a dilated cardiomyopathy which developed as the mice aged. Representative examples of echocardiograms in the 16-week-old control and cVclKO mice are shown in Fig. 5E and F. As mentioned above, we restricted our detailed analyses to male cVclKO mice, yet female mice also showed gross evidence of heart failure, with dilated hearts and accumulation of edema fluid evidenced by ascites, pericardial effusion, and increased lung weight (data not shown). Histologically, replacement fibrosis and left ventricular dilation were noted in the cVclKO mice compared to what was found for the controls (Fig. 5G and H).



Cardiac conduction abnormalities and ventricular tachycardia are seen in cVclKO mice at early ages. Since the cVclKO mice were found to have high mortality rates early in life despite normal systolic cardiac function, we next examined whether arrhythmias that could lead to sudden death might be present. For this purpose, we performed conscious telemetric monitoring of electrocardiograms. As shown in Fig. 6A, control mice showed evidence of normal sinus rhythm, with P waves preceding each narrow QRS complex. In contrast, cVclKO mice showed frequent evidence of heart block (Fig. 6B), and more dramatically, two of the three monitored cVclKO mice showed runs of polymorphic ventricular tachycardia (Fig. 6C).

To further evaluate the etiology of rhythm disturbances, electrical activity was monitored in the Langendorff-perfused hearts of 8-week-old cVclKO and control mice. We first analyzed hearts prior to dye loading or pacing. In this basal state, six of seven cVclKO hearts (86%) had spontaneous ventricular ectopy, while no ectopy was seen in seven control hearts (data not shown). Next, optical mapping was performed using the voltage-sensitive dye Di-4-ANEPPS. Action potential propagation was recorded during intrinsic rhythm and ventricular epicardial pacing. The electrical activity of the left ventricular epicardium was mapped with a high-speed charge-coupled-device camera, and activation patterns were analyzed. During apical pacing, cVclKO hearts displayed disturbed wave front propagation compared to controls ($n = 7$ for each group). Representative maps from one control and one KO heart are shown in Fig. 6D and E. Quantification of the map data showed a greater negative wave front curvature in the KO hearts than in the controls, which was consistent with an arrhythmogenic substrate ($-1.284 \pm 0.435 \text{ mm}^{-1}$ in cVclKO versus $-0.751 \pm 0.333 \text{ mm}^{-1}$ in controls; $P < 0.05$; $n = 7$ for each group). During point pacing, a positive wave front curvature is expected and a negative curvature indicates a region of local conduction slowing. These data were obtained from animals that did not have evidence of cardiac dysfunction, so the arrhythmogenic phenotype could be specifically analyzed distinct from the effects that cardiac dysfunction might have on rhythm generation. Separately, older KO hearts that had progressed to show a cardiomyopathic phenotype were shown to have similar optical maps and displayed frequent arrhythmias, while no rhythm abnormalities were seen in the control hearts (data not shown). These data importantly indicate that the cVclKO myocardium is prone to ventricular ectopy and lethal ventricular arrhythmias prior to the onset of functional abnormalities but, not surprisingly, continues to have this propensity as the cVclKO myocardium becomes dysfunctional. The combined data of conscious

telemetry and optical mapping show that vinculin deficiency severely disrupts electrical conduction in the heart prior to any changes in contractile dysfunction.

Vinculin deficiency results in abnormal myocardial ultrastructure prior to any changes in cardiac function. To determine if ultrastructural changes might be evident in the myocardium prior to any detectable change in physiological function, we evaluated myocardial samples from 6-week-old mice (Fig. 7A to D). Since vinculin is located at the ICD, and ICDs are critical regions for cell-cell stabilization within the myocardium, we particularly focused on this area of the tissue. Samples were obtained from five mice of each genotype and examined by a microscopist blinded to the genotype of the sample. Representative photomicrographs from the samples are shown. Control tissue showed electron-dense ICDs with contractile filaments inserted tightly into the region immediately juxtaposed to the ICD (Fig. 7A and C). In contrast, cVclKO samples showed a more highly serrated ICD structure which had reduced electron-dense staining throughout (Fig. 7B and D). Myofibrils also appeared separated from the ICD compared to what was found for the control samples (Fig. 7B and D). In addition, mitochondria were seen as tightly packed strands between myofibrillar structures in control hearts but were loosely arranged and disorganized in the cVclKO tissue. These results show that loss of vinculin from the cardiac myocyte disturbs ICDs, myofibrillar structure, and mitochondria prior to alterations in myocardial function. Alterations in the ICD could predispose the cVclKO mice toward both abnormal cardiac conduction and disturbed function, as shown above.

Loss of vinculin from myocytes correlates with reduced expression of cadherin and integrin from the myocardium as well as redistribution of connexin 43. To assess whether reduced myocyte vinculin might alter the expression or cellular arrangement of other proteins within cell-matrix or cell-cell adhesive junctions, we evaluated representative proteins found within these cellular sites. Western blotting was performed on whole-heart lysates and showed that both cadherin and the muscle-specific isoform of $\beta 1$ integrin ($\beta 1D$) were decreased in parallel with metavinculin reduction in the cVclKO hearts compared to control levels (Fig. 7E). No changes in protein expression levels of Cx43, desmoplakin, or α -catenin were noted (data not shown). Microscopy using the anti- $\beta 1D$ integrin antibody was in agreement with these Western blot results, as shown earlier in Fig. 2C. These results suggest that when vinculin/metavinculin is lost from the myocyte, altered expression of proteins within cell junctions occurs.

Immunomicroscopy was next performed on tissue from physiologically normal 8-week-old cVclKO and littermate

FIG. 6. Sudden arrhythmic death and conduction abnormalities are found in cVclKO mice prior to any decrement in systolic function. (A to C) Rhythm strips from conscious telemetry. Normal sinus rhythms were seen in control mice (A) compared to complete atrioventricular block and ectopy in cVclKO mice (B). Two of the three 13-week-old cVclKO mice showed nonsustained polymorphic ventricular tachycardia (C) and died soon after. (D and E) Optical mapping was performed on isolated mouse hearts. Optical mapping of the left ventricular epicardium was performed with 8-week-old control and cVclKO hearts. Epicardial pacing of control (D) and cVclKO (E) hearts was performed, and activation maps were constructed. Representative data are shown as was detected uniformly in all hearts tested from each group. cVclKO hearts displayed irregular conduction wave fronts, with regions of greater negative curvature indicating a region of local conduction slowing ($-1.284 \pm 0.435 \text{ mm}^{-1}$ in cVclKO versus $-0.751 \pm 0.333 \text{ mm}^{-1}$ in the control; $P < 0.05$; $n = 7$ for each group).

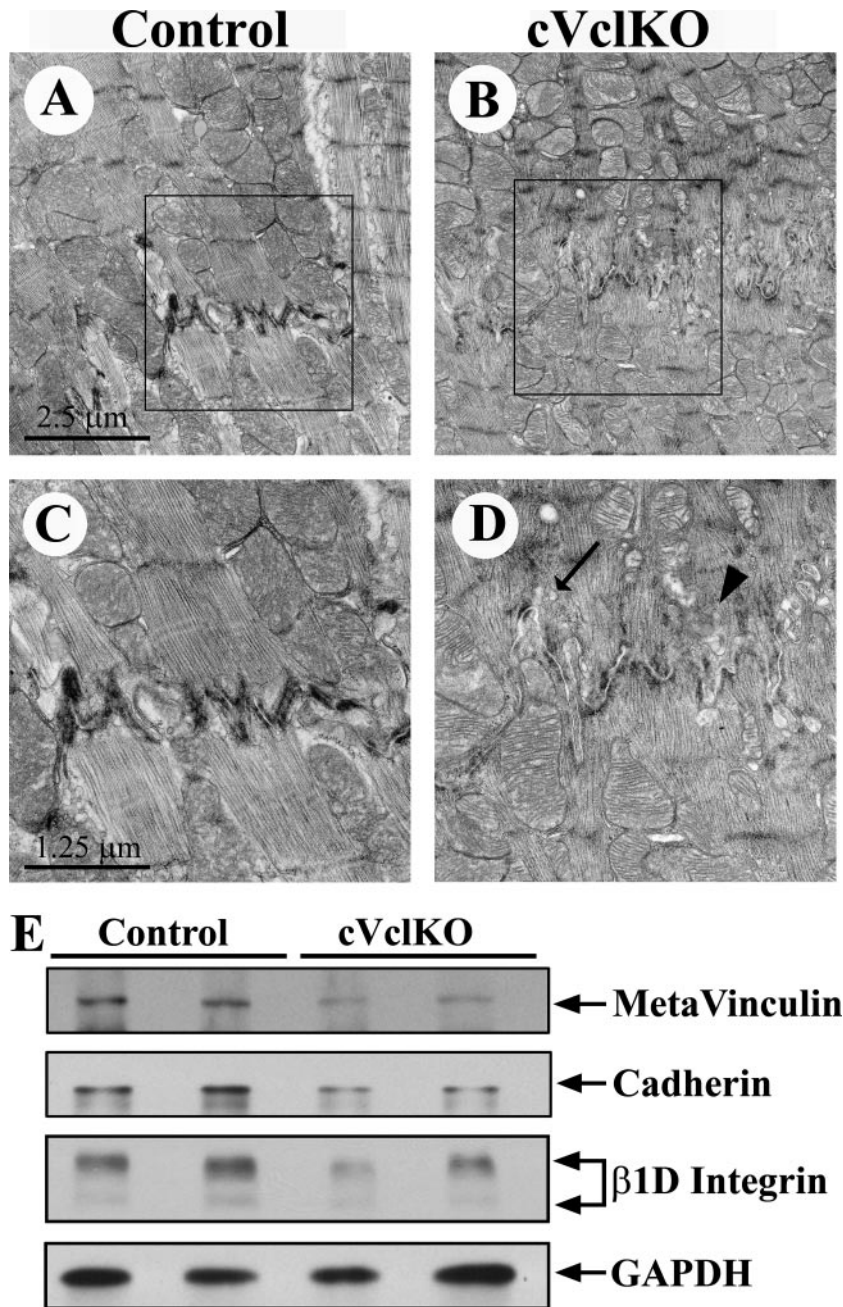


FIG. 7. cVclKO hearts show dissolution of the ICD structure and reduced expression of proteins in both cell-cell and cell-matrix junctions. (A to D) Ultrastructural morphology of left ventricular cardiac muscle from 6-week-old mice was analyzed. Control mice (A and C) showed well-aligned arrays and insertions of myofibrils at Z lines and preserved ICD structures. Mitochondria are visible in packed strands and are of normal size. In contrast, cVclKO samples (B and D) showed abnormal ICDs, with a reduced electro-density of the cell-to-cell contact site (arrow in panel D) and with increased separation of myofibrils at their insertion into the ICD (arrowhead in panel D). Additionally, disorganized and swollen mitochondria are seen in the cVclKO micrograph (B and D). Panels are representative of micrographs obtained from five animals of each genotype that were reviewed by investigators blinded to the genotype of the animal. (E) Whole-heart lysates from 12-week-old mice with preserved cardiac function were analyzed by Western blotting. Representative blots are shown. Densitometric analyses of cVclKO hearts showed a 71% reduction of metavinculin protein expression ($P < 0.007$, $n = 3$), 42% reduced protein expression of the muscle-specific integrin isoform β 1D, and 55% reduced cadherin protein expression compared to control levels ($P < 0.03$, $n = 3$) (data not shown). Densitometric analyses were performed by normalizing metavinculin, cadherin, or β 1D integrin expression to simultaneously measured GAPDH levels.

control hearts. Antibodies were chosen to detect each of the three junction types found within the ICD: adherens junctions (cadherin), gap junctions (connexin 43), and desmosomes (desmoplakin). Since residual vinculin expression can

be seen in the cVclKO myocardium, in each case we colocalized vinculin expression with the other protein of interest. As shown in Fig. 8A to C, cells which did not express vinculin similarly showed absent cadherin expression in

ICDs (Fig. 8A, panels 4 to 6). Cx43 expression, which was found mainly at the ICDs in control mice (Fig. 8B, panels 7 to 9), was redistributed to the lateral cell border in cVclKO cardiac myocytes (Fig. 8B, panels 10 to 12). Although cadherin as well as Cx43 immunostaining appeared abnormal in cVclKO hearts, the desmoplakin expression pattern was preserved in the ICD (Fig. 8C, panels 13 to 18). These data show that when vinculin is lost from cardiac myocytes, expression of the junctional proteins cadherin and β 1D integrin are reduced, and Cx43 becomes mislocalized to the lateral cell border.

DISCUSSION

The membrane-associated protein vinculin plays an important role in cell adhesion of cultured cells (13, 38, 63, 65). In whole-animal studies, global (total) KO of the vinculin gene caused lethality at embryonic day 10.5, with neurological and cardiac abnormalities (86). Vinculin's role in the intact heart was specifically tested in the current study. We created a mouse with a "floxed" Vcl allele. These mice were mated to ones where Cre recombinase was expressed only in cardiac myocytes, leading to cardiac-specific Vcl gene excision. This is the first report of mice with a "floxed" Vcl allele. This mouse model will allow *in vivo* excision of the Vcl gene in a cell- or tissue-specific manner. Further, our data directly link vinculin's *in vivo* function to preservation of normal cell-cell and cell-matrix adhesive structures of the cardiomyocyte.

We had hypothesized that vinculin would be critical for the mechanical stability of cardiac myocytes, since it is an actin-binding protein positioned for anchoring the sarcomere to the cell membrane as well as one myocyte to the next. In line with this, we found that 49% of the cVclKO mice appeared initially healthy but died suddenly before 14 weeks of age, while mice that survived past this age developed cardiac dysfunction. Given these physiological findings, we investigated the protein expression and localization of components from all three ICD junctions in 8-week-old cVclKO mice. We particularly chose to study mice at this young age since they showed only minimal abnormalities in physiological function. Once hearts have evolved to show compromised function (heart failure), many secondary abnormalities can result and it can be difficult to link pathological abnormalities with a primary protein abnormality.

Reduced cadherin expression and disturbed ICDs in cVclKO mice. In our young cVclKO mice, the adherens junction protein N-cadherin was shown absent from vinculin-null cardiac myocytes. At the ultrastructural level, cVclKO mice showed altered ICD structures with deeply serrated cell-to-cell borders and reduced electron-dense adherens junctions. In line with our finding were those for cardiac-specific N-cadherin KO mice which showed that the loss of myocyte N-cadherin resulted in the destabilization of the ICD as well as gap junctions, leading to disturbed electrical function (41, 43). It is interesting to note that vinculin directly binds α -catenin and that catenins are tightly linked to cadherins. In contrast to the phenotype in the N-cadherin cKO mice, cardiac-specific excision of α -E catenin showed right ventricular thinning and left ventricular dilation in the

absence of any arrhythmias. Vinculin was completely lost from ICDs in these mice. Several studies of cardiac-specific β -catenin KO mice found no phenotype, likely due to up-regulation of the related protein plakoglobin (67, 89), though recent work showed that loss of β -catenin from myocytes may cause adaptive hypertrophy in the adult heart (5). In addition, cardiac-specific expression of a stabilized mutant of β -catenin prevented angiotensin II-induced cardiac hypertrophy (5).

Our study shows that loss of vinculin dramatically alters cadherin-containing cell-to-cell adhesion structures, leading to destruction of ICDs. The mechanism of how vinculin precisely controls the expression levels of cadherin and more importantly stabilizes the adherens junction can only be conjectured. A traditional view has been that vinculin is part of the large and growing complex of proteins which couple cadherin, through catenins, to the actin filaments within the cell (26). Recent work by the Weis and Nelson groups (22, 80, 87) have called this stabilized view of the cadherin-based junction into question and suggest one where there are dynamic changes in α -catenin to regulate the actin-based cytoskeleton. Interestingly, at least in the model system used by these authors (22, 87), vinculin could not bind to the cadherin- β -catenin complex and actin at the same time. As we found evidence for in the whole heart, loss of vinculin from all locations within the myocyte likely effects tension development in the cell. Interestingly, work with COS-7 and MTD-1A cells (48) showed that inhibition of cell tension through RNA interference suppression of myosin II or treatment with blebbistatin directly caused loss of vinculin from the cells but did not affect the cadherin/catenin complex localization.

Vinculin is also localized in the cell-cell adherens junctions that link one cell to the next (27, 28). In binding to catenins, it is recruited to the tails of cadherins and thereby is detected in the adherens junctions (81). Recent work has shown that vinculin regulates association of β -catenin with membrane-associated guanylate-kinase inverted 2 (MAGI-2). In turn, PTEN, a tumor suppressor, is reduced by ubiquitin proteolytic degradation (70). Related work on MAGI-1 in endothelial cells showed that with MAGI-1 depletion, vinculin redistributed from cell-matrix to cell-cell adhesions and that vinculin might be part of a feedback loop which could strengthen adherens junctions (61). Thereby, vinculin appears to play a critical role in the dynamic regulation of adherens junctions, at least in epithelial and endothelial cells, and based on our data, is also essential for preservation of adherens junctions in cardiac myocytes.

Heterogeneous Cx43 distribution in young cVclKO mice. Rapid communication between myocytes requires gap junctions, one component of the ICD. In our cVclKO mice, we found a redistribution of Cx43 from the ICD to the lateral cell wall in the vinculin-null cells. As is the case in many Cre-Lox mouse models, there were still some myocytes which continued to express vinculin, and therefore, they also displayed normal Cx43 distribution. Therefore, cVclKO heart tissue has heterogeneous Cx43 distribution, which in itself might predispose toward cardiac rhythm disturbance. In support of our findings, heterogeneous KO of Cx43 in a chimeric mouse model resulted in localized regions of cell-

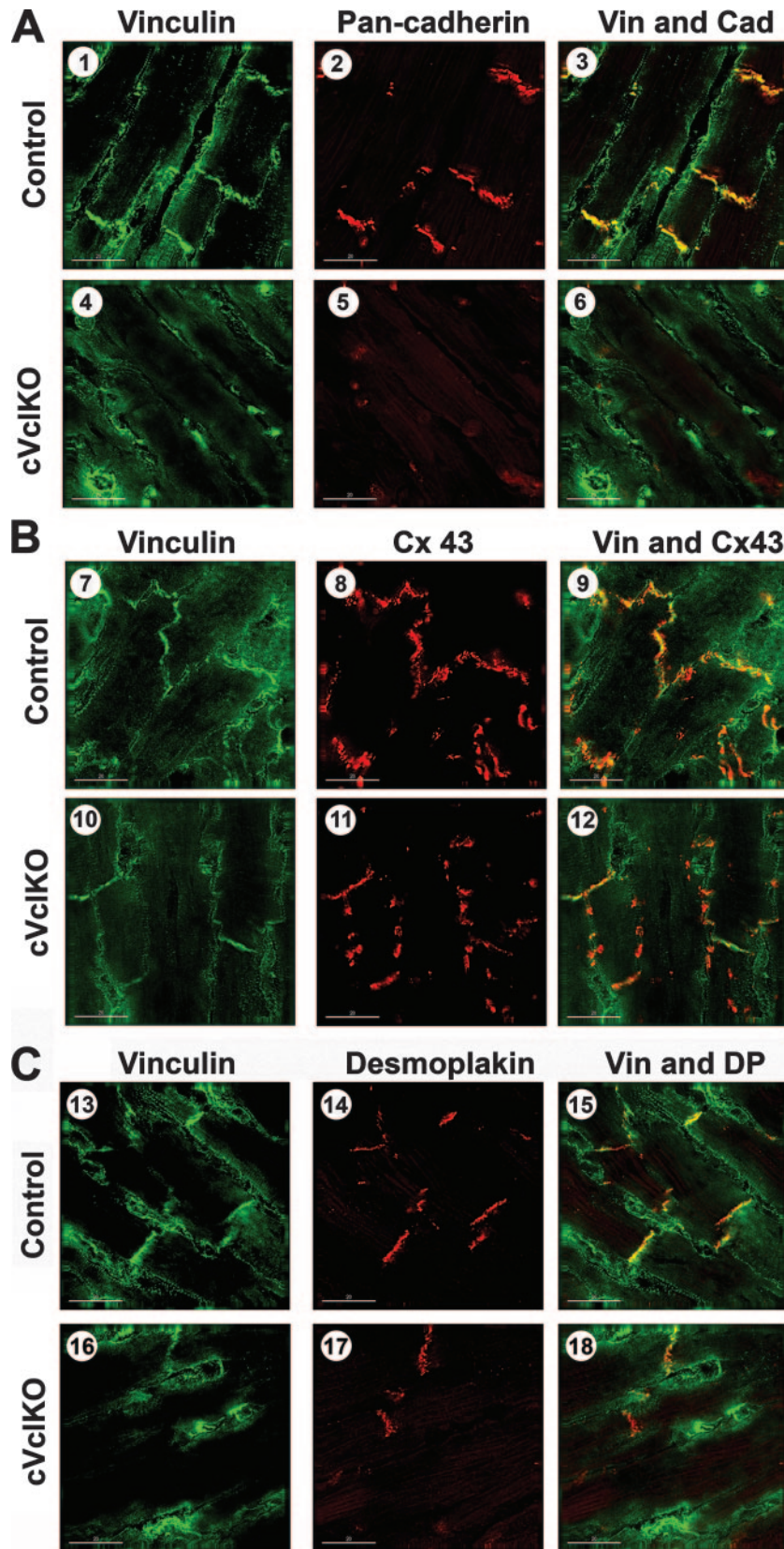


FIG. 8. Cardiac myocytes null for vinculin (Vin) show lack of cadherin (Cad) expression and abnormal distribution of connexin 43. Tissue from physiologically normal cVclKO and control hearts was obtained at 8 weeks of age and examined by deconvolution microscopy. Immunofluorescence was performed using a series of antibodies representative of all three major junctions of the ICD. All pictures represent a 2.5- μ m Z stack from

cell uncoupling, leading to disturbed activation wave front curvature and development of spontaneous arrhythmias (37). Since, in the adult heart, Cx43 usually localizes in the end-to-end junctional complexes forming low-resistance pathways for propagation of electrical impulses between cardiomyocytes, an altered distribution, as we saw in the cVclKO mice, likely provided for an arrhythmogenic substrate (1). Concordant with our findings of ventricular rhythm disturbances in the cVclKO mice, patients with chronic atrial fibrillation showed lateralization of Cx in atrial tissue (56).

At the ICD, Cx43 is associated with an N-cadherin-containing multiprotein complex that is required for gap junction formation, although some studies suggest that the organization of adherens junctions and desmosomes is independent of gap junctions (35). To our knowledge, vinculin has not been shown to directly bind Cx43 (31). Studies of liver and NIH 3T3 cells have suggested that cadherins are essential for gap junction formation (24, 43, 79). Further, work using neonatal rat cardiac myocytes indicated a role for catenins in development of gap junctions (85). Elegant recent work using HeLa cells showed that small interfering RNA knock-down of β -catenin or disruption of cadherin interactions with the adherens junction could disrupt gap junction formation, in line with models indicating that gap junction formation is preceded by cell-cell contact and hemophilic cadherin-cadherin interactions (66). In agreement with our data, cardiac-myocyte-specific loss of N-cadherin led to decreased Cx43 expression levels, with conduction slowing and arrhythmogenesis (43). Further, induction of myocardial infarction in rats led to combined mislocalization of adherens and gap junctions (46), while an ischemia-reperfusion stress in rabbit hearts led to reduction and redistribution of both N-cadherin and Cx43, with the loss of cadherin preceding that of the connexin (72). Still, how adherens and gap junctions functionally interact is not completely understood (60). Mice with cardiac-myocyte-specific loss of Cx43 have normal heart structure and contractile performance but, similar to our cVclKO model, show spontaneous ventricular arrhythmias and sudden death (36). Studies of astrocytes have shown that increased pressure can cause loss of membrane-associated Cx43 with redistribution of the connexin protein in the cytoplasm (45). Our young vinculin-deficient hearts had only minor changes in relaxation, with no other significant physiological changes. Therefore, it is unlikely that Cx43 distribution in the young cVclKO hearts was affected by physical changes, as was shown in astrocytes. Still, further studies are necessary to show whether loss of vinculin from the multiprotein complex which includes cadherins

and catenins directly causes altered distribution of connexins in our model.

In their basal "unstressed" state, young cVclKO mice showed evidence of mild morphometric, histological, and molecular cardiac hypertrophy. Invasive catheterization revealed normal baseline systolic function that responded appropriately to adrenergic agonist stimulation, though dP/dt_{min} , an indicator of relaxation, was found to be abnormal during administration of dobutamine. These abnormalities are consistent with restrictive cardiac physiology. Restrictive cardiomyopathy is rare and often associated with sudden death in children, but the underlying mechanism has not been determined (30, 57).

Dilated cardiomyopathy develops in cVclKO mice older than 3 months of age. The structural integrity of the myocyte and whole heart requires proper mechanical linkages between cells, as would be orchestrated by adherens junctions, as well as from cells to the extracellular matrix, provided by the costameric complex. cVclKO mice that survived through the vulnerable period of sudden death developed dilated cardiomyopathy and died before 6 months of age. When we examined young mice that did not yet have functional abnormalities, we found loss of both cadherin expression and the costameric protein β 1 integrin. Since vinculin serves roles in both of these critical structural linkages of the heart, the vinculin-deficient myocyte can clearly be predisposed toward failure. Interestingly, mice with cardiac-specific deletion of the costameric proteins integrin-linked kinase, β 1 integrin, focal adhesion kinase, and Melusin all displayed a dilated cardiomyopathic phenotype, though some of these models required a second "hit" of either pharmacological or hemodynamic stress for this to occur (11, 21, 53, 64, 83). Importantly, in agreement with our tenet that the localization of vinculin at the ICD predisposes the cVclKO mice to cardiac arrhythmias, none of these mouse models with only costameric protein disturbances had an arrhythmogenic phenotype preceding the development of heart failure.

In conclusion, we have developed the first model which allows assessment of vinculin's function in a tissue/cell-specific manner. In the heart, vinculin deficiency leads to destabilization of the cadherin-catenin protein complex, maldistribution of gap junction proteins, and disturbance of cell-matrix junctional proteins. Therefore, normal vinculin expression is necessary for preservation of both contractile and electrical function. The dilated cardiomyopathic phenotype of our model agrees with that seen in patients with metavinclulin mutations. Our results suggest that genetic screening for vinculin mutations in patients with family histories of lethal cardiac arrhythmias or cardiac dysfunction is prudent.

five individual 0.5- μ m sections. Since residual vinculin expression could still be detected in the cVclKO hearts, immunofluorescent staining with an antivinculin antibody was performed in all examinations. cVclKO hearts showed absent vinculin staining at costameres and ICDs compared to normal vinculin distribution in control hearts (A, panels 1 and 4; B, panels 7 and 10; and C, panels 13 and 16). Pan-cadherin staining was localized normally in the control ICDs (A, panels 2 and 3) but was absent in cVclKO cardiac myocytes (A, panels 5 and 6). Cx43 staining was localized along the ICD region in the control (B, panels 8 and 9) but was redistributed to the lateral cell border in cVclKO myocytes (B, panels 11 and 12). Desmoplakin (DP) staining was found to be normally localized in control ICDs (C, panels 14 and 15) as well as in cVclKO (C, panels 17 and 18). (A) Vinculin (green) and pan-cadherin (red) staining in control and cVclKO hearts. (B) Vinculin (green) and Cx43 (red) staining in control and cVclKO hearts. (C) Vinculin (green) and desmoplakin (red) staining in control and cVclKO hearts.

ACKNOWLEDGMENTS

We thank Ju Chen and Kirk Knowlton as well as members of the Ross, Chen, and Knowlton laboratories for helpful criticisms and Steve Padilla for expert technical assistance. Jon Seidman and Paul Clopton provided useful discussion on statistical analyses.

This work was supported by NIH grants HL57872 and HL73393 and a Veterans Administration Merit Award to R.S.R. A.D.M. was supported by NIH grant HL46345 and NSF grant BES-0506252. A portion of the work was performed in UCSD's NCMIR, supported by P41-R004050 from NIH.

REFERENCES

- Angst, B. D., L. U. Khan, N. J. Severs, K. Whitely, S. Rothery, R. P. Thompson, A. I. Magee, and R. G. Gourdie. 1997. Dissociated spatial patterning of gap junctions and cell adhesion junctions during postnatal differentiation of ventricular myocardium. *Circ. Res.* **80**:88–94.
- Babbitt, C. J., S. Y. Shai, A. E. Harpf, C. G. Pham, and R. S. Ross. 2002. Modulation of integrins and integrin signaling molecules in the pressure-loaded murine ventricle. *Histochem. Cell Biol.* **118**:431–439.
- Bakolitsa, C., D. M. Cohen, L. A. Bankston, A. A. Bobkov, G. W. Cadwell, L. Jennings, D. R. Critchley, S. W. Craig, and R. C. Liddington. 2004. Structural basis for vinculin activation at sites of cell adhesion. *Nature* **430**:583–586.
- Barstead, R. J., and R. H. Waterston. 1991. Vinculin is essential for muscle function in the nematode. *J. Cell Biol.* **114**:715–724.
- Baurand, A., L. Zelarayan, R. Betney, C. Gehrke, S. Dunger, C. Noack, A. Busjahn, J. Huelsken, M. M. Taketo, W. Birchmeier, R. Dietz, and M. W. Bergmann. 2007. Beta-catenin downregulation is required for adaptive cardiac remodeling. *Circ. Res.* **100**:1353–1362.
- Bayly, P. V., B. H. KenKnight, J. M. Rogers, R. E. Hillsley, R. E. Ideker, and W. M. Smith. 1998. Estimation of conduction velocity vector fields from epicardial mapping data. *IEEE Trans. Biomed. Eng.* **45**:563–571.
- Belkin, A. M., O. I. Ornatsky, M. A. Glukhova, and V. E. Koteliansky. 1988. Immunolocalization of meta-vinculin in human smooth and cardiac muscles. *J. Cell Biol.* **107**:545–553.
- Belkin, A. M., O. I. Ornatsky, A. E. Kabakov, M. A. Glukhova, and V. E. Koteliansky. 1988. Diversity of vinculin/meta-vinculin in human tissues and cultivated cells. Expression of muscle specific variants of vinculin in human aorta smooth muscle cells. *J. Biol. Chem.* **263**:6631–6635.
- Birks, E. J., J. L. Hall, P. J. Barton, S. Grindle, N. Latif, J. P. Hardy, J. E. Rider, N. R. Banner, A. Khaghani, L. W. Miller, and M. H. Yacoub. 2005. Gene profiling changes in cytoskeletal proteins during clinical recovery after left ventricular-assist device support. *Circulation* **112**:157–164.
- Borgon, R. A., C. Vonrhein, G. Bricogne, P. R. Bois, and T. Izard. 2004. Crystal structure of human vinculin. *Structure* **12**:1189–1197.
- Brancaccio, M., L. Fratta, A. Notte, E. Hirsch, R. Poulet, S. Guazzone, M. De Acetis, C. Vecchione, G. Marino, F. Altruda, L. Silengo, G. Tarone, and G. Lembo. 2003. Melusin, a muscle-specific integrin beta1-interacting protein, is required to prevent cardiac failure in response to chronic pressure overload. *Nat. Med.* **9**:68–75.
- Byrne, B. J., Y. J. Kaczorowski, M. D. Coutu, and S. W. Craig. 1992. Chicken vinculin and meta-vinculin are derived from a single gene by alternative splicing of a 207-base pair exon unique to meta-vinculin. *J. Biol. Chem.* **267**:12845–12850.
- Chen, H., D. M. Cohen, D. M. Choudhury, N. Kioka, and S. W. Craig. 2005. Spatial distribution and functional significance of activated vinculin in living cells. *J. Cell Biol.* **169**:459–470.
- Chen, J., S. W. Kubalak, S. Minamisawa, R. L. Price, K. D. Becker, R. Hickey, J. J. Ross, and K. R. Chien. 1998. Selective requirement of myosin light chain 2v in embryonic heart function. *J. Biol. Chem.* **273**:1252–1256.
- Chopard, A., F. Pons, and J. F. Marini. 2002. Vinculin and meta-vinculin in fast and slow rat skeletal muscle before and after hindlimb suspension. *Pflugers Arch.* **444**:627–633.
- Clark, K. A., A. S. McElhinny, M. C. Beckerle, and C. C. Gregorio. 2002. Striated muscle cytoarchitecture: an intricate web of form and function. *Annu. Rev. Cell Dev. Biol.* **18**:637–706.
- Cohen, D. M., B. Kutscher, H. Chen, D. B. Murphy, and S. W. Craig. 2006. A conformational switch in vinculin drives formation and dynamics of a talin-vinculin complex at focal adhesions. *J. Biol. Chem.* **281**:16006–16015.
- Critchley, D. R. 2004. Cytoskeletal proteins talin and vinculin in integrin-mediated adhesion. *Biochem. Soc. Trans.* **32**:831–836.
- Crone, S. A., Y. Y. Zhao, L. Fan, Y. Gu, S. Minamisawa, Y. Liu, K. L. Peterson, J. Chen, R. Kahn, G. Condorelli, J. Ross, Jr., K. R. Chien, and K. F. Lee. 2002. ErbB2 is essential in the prevention of dilated cardiomyopathy. *Nat. Med.* **8**:459–465.
- Demali, K. A. 2004. Vinculin—a dynamic regulator of cell adhesion. *Trends Biochem. Sci.* **29**:565–567.
- DiMichele, L. A., J. T. Doherty, M. Rojas, H. E. Beggs, L. F. Reichardt, C. P. Mack, and J. M. Taylor. 2006. Myocyte-restricted focal adhesion kinase deletion attenuates pressure overload-induced hypertrophy. *Circ. Res.* **99**:636–645.
- Drees, F., S. Pokutta, S. Yamada, W. J. Nelson, and W. I. Weis. 2005. Alpha-catenin is a molecular switch that binds E-cadherin-beta-catenin and regulates actin-filament assembly. *Cell* **123**:903–915.
- Ezzell, R. M., W. H. Goldmann, N. Wang, N. Parasharama, and D. E. Ingber. 1997. Vinculin promotes cell spreading by mechanically coupling integrins to the cytoskeleton. *Exp. Cell Res.* **231**:14–26.
- Fujimoto, K., A. Nagafuchi, S. Tsukita, A. Kuraoka, A. Ohokuma, and Y. Shibata. 1997. Dynamics of connexins, E-cadherin and alpha-catenin on cell membranes during gap junction formation. *J. Cell Sci.* **110**:311–322.
- Gallant, N. D., K. E. Michael, and A. J. Garcia. 2005. Cell adhesion strengthening: contributions of adhesive area, integrin binding, and focal adhesion assembly. *Mol. Biol. Cell* **16**:4329–4340.
- Gates, J., and M. Peifer. 2005. Can 1000 reviews be wrong? Actin, alpha-catenin, and adherens junctions. *Cell* **123**:769–772.
- Geiger, B., A. H. Dutton, K. T. Tokuyasu, and S. J. Singer. 1981. Immunoelectron microscope studies of membrane-microfilament interactions: distributions of alpha-actinin, tropomyosin, and vinculin in intestinal epithelial brush border and chicken gizzard smooth muscle cells. *J. Cell Biol.* **91**:614–628.
- Geiger, B., K. T. Tokuyasu, A. H. Dutton, and S. J. Singer. 1980. Vinculin, an intracellular protein localized at specialized sites where microfilament bundles terminate at cell membranes. *Proc. Natl. Acad. Sci. USA* **77**:4127–4131.
- Geiger, B., T. Volk, and T. Volberg. 1985. Molecular heterogeneity of adherens junctions. *J. Cell Biol.* **101**:1523–1531.
- Gewillig, M., L. Mertens, P. Moerman, and M. Dumoulin. 1996. Idiopathic restrictive cardiomyopathy in childhood. A diastolic disorder characterized by delayed relaxation. *Eur. Heart J.* **17**:1413–1420.
- Giepmans, B. N. 2004. Gap junctions and connexin-interacting proteins. *Cardiovasc. Res.* **62**:233–245.
- Gilmore, A. P., and K. Burridge. 1996. Regulation of vinculin binding to talin and actin by phosphatidylinositol-4-5-bisphosphate. *Nature* **381**:531–535.
- Gingras, A. R., K. P. Vogel, H. J. Steinhoff, W. H. Ziegler, B. Patel, J. Emsley, D. R. Critchley, G. C. Roberts, and I. L. Barsukov. 2006. Structural and dynamic characterization of a vinculin binding site in the talin rod. *Biochemistry* **45**:1805–1817.
- Goldmann, W. H., R. Galneder, M. Ludwig, W. Xu, E. D. Adamson, N. Wang, and R. M. Ezzell. 1998. Differences in elasticity of vinculin-deficient F9 cells measured by magnetometry and atomic force microscopy. *Exp. Cell Res.* **239**:235–242.
- Gutstein, D. E., F. Y. Liu, M. B. Meyers, A. Choo, and G. I. Fishman. 2003. The organization of adherens junctions and desmosomes at the cardiac intercalated disc is independent of gap junctions. *J. Cell Sci.* **116**:875–885.
- Gutstein, D. E., G. E. Morley, H. Tamaddon, D. Vaidya, M. D. Schneider, J. Chen, K. R. Chien, H. Stuhlmann, and G. I. Fishman. 2001. Conduction slowing and sudden arrhythmic death in mice with cardiac-restricted inactivation of connexin43. *Circ. Res.* **88**:333–339.
- Gutstein, D. E., G. E. Morley, D. Vaidya, F. Liu, F. L. Chen, H. Stuhlmann, and G. I. Fishman. 2001. Heterogeneous expression of Gap junction channels in the heart leads to conduction defects and ventricular dysfunction. *Circulation* **104**:1194–1199.
- Hu, K., L. Ji, K. T. Applegate, G. Danuser, and C. M. Waterman-Storer. 2007. Differential transmission of actin motion within focal adhesions. *Science* **315**:111–115.
- Izard, T., G. Evans, R. A. Borgon, C. L. Rush, G. Bricogne, and P. R. Bois. 2004. Vinculin activation by talin through helical bundle conversion. *Nature* **427**:171–175.
- Janssen, M. E., E. Kim, H. Liu, L. M. Fujimoto, A. Bobkov, N. Volkman, and D. Hanein. 2006. Three-dimensional structure of vinculin bound to actin filaments. *Mol. Cell* **21**:271–281.
- Kostetskii, I., J. Li, Y. Xiong, R. Zhou, V. A. Ferrari, V. V. Patel, J. D. Molkentin, and G. L. Radice. 2005. Induced deletion of the N-cadherin gene in the heart leads to dissolution of the intercalated disc structure. *Circ. Res.* **96**:346–354.
- Koteliansky, V. E., E. P. Ogrzyko, N. I. Zhidkova, P. A. Weller, D. R. Critchley, K. Vancompernelle, J. Vandekerckhove, P. Strasser, M. Way, and M. Gimona. 1992. An additional exon in the human vinculin gene specifically encodes meta-vinculin-specific difference peptide. Cross-species comparison reveals variable and conserved motifs in the meta-vinculin insert. *Eur. J. Biochem.* **205**:1218.
- Li, J., V. V. Patel, I. Kostetskii, Y. Xiong, A. F. Chu, J. T. Jacobson, C. Yu, G. E. Morley, J. D. Molkentin, and G. L. Radice. 2005. Cardiac-specific loss of N-cadherin leads to alteration in connexins with conduction slowing and arrhythmogenesis. *Circ. Res.* **97**:474–481.
- Maeda, M., E. Holder, B. Lowes, S. Valent, and R. D. Bies. 1997. Dilated cardiomyopathy associated with deficiency of the cytoskeletal protein meta-vinculin. *Circulation* **95**:17–20.
- Malone, P., H. Miao, A. Parker, S. Juarez, and M. R. Hernandez. 2007. Pressure induces loss of gap junction communication and redistribution of connexin 43 in astrocytes. *Glia* **55**:1085–1098.

46. Matsushita, T., M. Oyamada, K. Fujimoto, Y. Yasuda, S. Masuda, Y. Wada, T. Oka, and T. Takamatsu. 1999. Remodeling of cell-cell and cell-extracellular matrix interactions at the border zone of rat myocardial infarcts. *Circ. Res.* **85**:1046–1055.
47. Melo, T. G., D. S. Almeida, M. N. de Meirelles, and M. C. Pereira. 2004. Trypanosoma cruzi infection disrupts vinculin costameres in cardiomyocytes. *Eur. J. Cell Biol.* **83**:531–540.
48. Miyake, Y., N. Inoue, K. Nishimura, N. Kinoshita, H. Hosoya, and S. Yonemura. 2006. Actomyosin tension is required for correct recruitment of adherens junction components and zonula occludens formation. *Exp. Cell Res.* **312**:1637–1650.
49. Moiseyeva, E. P., P. A. Weller, N. I. Zhidkova, E. B. Corben, B. Patel, I. Jasinska, V. E. Kotelianskiy, and D. R. Critchley. 1993. Organization of the human gene encoding the cytoskeletal protein vinculin and the sequence of the vinculin promoter. *J. Biol. Chem.* **268**:4318–4325.
50. O'Connell, T. D., M. C. Rodrigo, and P. C. Simpson. 2006. Isolation and culture of adult mouse cardiac myocytes, p. 271–296. *In* F. Vivanco (ed.), Cardiovascular proteomics: methods and protocols. Humana Press, Totowa, NJ.
51. Olson, T. M., S. Illenberger, N. Y. Kishimoto, S. Huttelmaier, M. T. Keating, and B. M. Jockusch. 2002. Metavinculin mutations alter actin interaction in dilated cardiomyopathy. *Circulation* **105**:431–437.
52. Pardo, J. V., J. D. Siliciano, and S. W. Craig. 1983. Vinculin is a component of an extensive network of myofibril-sarcolemma attachment regions in cardiac muscle fibers. *J. Cell Biol.* **97**:1081–1088.
53. Peng, X., M. S. Kraus, H. Wei, T. L. Chen, R. Pariaut, A. Alcaraz, G. Ji, L. Cheng, Q. Yang, M. I. Kotlikoff, J. Chen, K. Chien, H. Gu, and J. L. Guan. 2006. Inactivation of focal adhesion kinase in cardiomyocytes promotes eccentric cardiac hypertrophy and fibrosis in mice. *J. Clin. Investig.* **116**:217–227.
54. Perriard, J. C., A. Hirschy, and E. Ehler. 2003. Dilated cardiomyopathy: a disease of the intercalated disc? *Trends Cardiovasc. Med.* **13**:30–38.
55. Pham, C. G., A. E. Harpf, R. S. Keller, H. T. Vu, S. Y. Shai, J. C. Loftus, and R. S. Ross. 2000. Striated muscle-specific beta(1D)-integrin and FAK are involved in cardiac myocyte hypertrophic response pathway. *Am. J. Physiol. Heart Circ. Physiol.* **279**:H2916–H2926.
56. Polontchouk, L., J. A. Haefliger, B. Ebel, T. Schaefer, D. Stuhlmann, U. Mehlhorn, F. Kuhn-Regnier, E. R. De Vivie, and S. Dhein. 2001. Effects of chronic atrial fibrillation on gap junction distribution in human and rat atria. *J. Am. Coll. Cardiol.* **38**:883–891.
57. Rivenes, S. M., D. L. Kearney, E. O. Smith, J. A. Towbin, and S. W. Denfield. 2000. Sudden death and cardiovascular collapse in children with restrictive cardiomyopathy. *Circulation* **102**:876–882.
58. Rodriguez, C. I., F. Buchholz, J. Galloway, R. Sequerra, J. Kasper, R. Ayala, A. F. Stewart, and S. M. Dymecki. 2000. High-efficiency deleter mice show that FLPe is an alternative to Cre-loxP. *Nat. Genet.* **25**:139–140.
59. Rudiger, M., N. Korneeva, C. Schwienbacher, E. E. Weiss, and B. M. Jockusch. 1998. Differential actin organization by vinculin isoforms: implications for cell type-specific microfilament anchorage. *FEBS Lett.* **431**:49–54.
60. Saffitz, J. E., and A. G. Kleber. 2004. Effects of mechanical forces and mediators of hypertrophy on remodeling of gap junctions in the heart. *Circ. Res.* **94**:585–591.
61. Sakurai, A., S. Fukuhara, A. Yamagishi, K. Sako, Y. Kamioka, M. Masuda, Y. Nakaoka, and N. Mochizuki. 2006. MAGI-1 is required for Rap1 activation upon cell-cell contact and for enhancement of vascular endothelial cadherin-mediated cell adhesion. *Mol. Biol. Cell* **17**:966–976.
62. Samarel, A. M. 2005. Costameres, focal adhesions, and cardiomyocyte mechano-transduction. *Am. J. Physiol. Heart Circ. Physiol.* **289**:H2291–H2301.
63. Saunders, R. M., M. R. Holt, L. Jennings, D. H. Sutton, I. L. Barsukov, A. Bobkov, R. C. Liddington, E. A. Adamson, G. A. Dunn, and D. R. Critchley. 2006. Role of vinculin in regulating focal adhesion turnover. *Eur. J. Cell Biol.* **85**:487–500.
64. Shai, S. Y., A. E. Harpf, C. J. Babbitt, M. C. Jordan, M. C. Fishbein, J. Chen, M. Omura, T. A. Leil, K. D. Becker, M. Jiang, D. J. Smith, S. R. Cherry, J. C. Loftus, and R. S. Ross. 2002. Cardiac myocyte-specific excision of the beta1 integrin gene results in myocardial fibrosis and cardiac failure. *Circ. Res.* **90**:458–464.
65. Sharp, W. W., D. G. Simpson, T. K. Borg, A. M. Samarel, and L. Terracio. 1997. Mechanical forces regulate focal adhesion and costamere assembly in cardiac myocytes. *Am. J. Physiol.* **273**:H546–H556.
66. Shaw, R. M., A. J. Fay, M. A. Puthenvedu, M. von Zastrow, Y. N. Jan, and L. Y. Jan. 2007. Microtubule plus-end-tracking proteins target gap junctions directly from the cell interior to adherens junctions. *Cell* **128**:547–560.
67. Sheikh, F., Y. Chen, X. Liang, A. Hirschy, A. E. Stenbit, Y. Gu, N. D. Dalton, T. Yajima, Y. Lu, K. U. Knowlton, K. L. Peterson, J. C. Perriard, and J. Chen. 2006. alpha-E-catenin inactivation disrupts the cardiomyocyte adherens junction, resulting in cardiomyopathy and susceptibility to wall rupture. *Circulation* **114**:1046–1055.
68. Shiraishi, I., D. G. Simpson, W. Carver, R. Price, T. Hirozane, L. Terracio, and T. K. Borg. 1997. Vinculin is an essential component for normal myofibrillar arrangement in fetal mouse cardiac myocytes. *J. Mol. Cell. Cardiol.* **29**:2041–2052.
69. Siliciano, J. D., and S. W. Craig. 1982. Meta-vinculin—a vinculin-related protein with solubility properties of a membrane protein. *Nature* **300**:533–535.
70. Subauste, M. C., P. Nalbant, E. D. Adamson, and K. M. Hahn. 2005. Vinculin controls PTEN protein level by maintaining the interaction of the adherens junction protein beta-catenin with the scaffolding protein MAGI-2. *J. Biol. Chem.* **280**:5676–5681.
71. Sung, D., J. S. J. P. Cosman, R. Mills, and A. D. McCulloch. 2001. Phase shifting prior to spatial filtering enhances optical recordings of cardiac action potential propagation. *Ann. Biomed. Eng.* **29**:854–861.
72. Tansey, E. E., K. F. Kwaku, P. E. Hamner, D. B. Cowan, M. Federman, S. Levitsky, and J. D. McCully. 2006. Reduction and redistribution of gap and adherens junction proteins after ischemia and reperfusion. *Ann. Thorac. Surg.* **82**:1472–1479.
73. Terracio, L., D. G. Simpson, L. Hilenski, W. Carver, R. S. Decker, N. Vinson, and T. K. Borg. 1990. Distribution of vinculin in the Z-disk of striated muscle: analysis by laser scanning confocal microscopy. *J. Cell. Physiol.* **145**:78–87.
74. Thibault, G., M. J. Lacombe, L. M. Schnapp, A. Lacasse, F. Bouzeghrane, and G. Lapalme. 2001. Upregulation of alpha(8)beta(1)-integrin in cardiac fibroblast by angiotensin II and transforming growth factor-beta1. *Am. J. Physiol. Cell Physiol.* **281**:C1457–C1467.
75. Tokuyasu, K. T., A. H. Dutton, B. Geiger, and S. J. Singer. 1981. Ultrastructure of chicken cardiac muscle as studied by double immunolabeling in electron microscopy. *Proc. Natl. Acad. Sci. USA* **78**:7619–7623.
76. Vasile, V. C., S. R. Ommen, W. D. Edwards, and M. J. Ackerman. 2006. A missense mutation in a ubiquitously expressed protein, vinculin, confers susceptibility to hypertrophic cardiomyopathy. *Biochem. Biophys. Res. Commun.* **345**:998–1003.
77. Vasile, V. C., M. L. Will, S. R. Ommen, W. D. Edwards, T. M. Olson, and M. J. Ackerman. 2006. Identification of a metavinculin missense mutation, R975W, associated with both hypertrophic and dilated cardiomyopathy. *Mol. Genet. Metab.* **87**:169–174.
78. Volk, T., and B. Geiger. 1984. A 135-kd membrane protein of intercellular adherens junctions. *EMBO J.* **3**:2249–2260.
79. Wei, C. J., R. Francis, X. Xu, and C. W. Lo. 2005. Connexin43 associated with an N-cadherin-containing multiprotein complex is required for gap junction formation in NIH3T3 cells. *J. Biol. Chem.* **280**:19925–19936.
80. Weis, W. I., and W. J. Nelson. 2006. Re-solving the cadherin-catenin-actin conundrum. *J. Biol. Chem.* **281**:35593–35597.
81. Weiss, E. E., M. Kroemker, A. H. Rudiger, B. M. Jockusch, and M. Rudiger. 1998. Vinculin is part of the cadherin-catenin junctional complex: complex formation between alpha-catenin and vinculin. *J. Cell Biol.* **141**:755–764.
82. Weller, P. A., E. P. Ogryzko, E. B. Corben, N. I. Zhidkova, B. Patel, G. J. Price, N. K. Spurr, V. E. Kotelianskiy, and D. R. Critchley. 1990. Complete sequence of human vinculin and assignment of the gene to chromosome 10. *Proc. Natl. Acad. Sci. USA* **87**:5667–5671.
83. White, D. E., P. Coutu, Y. F. Shi, J. C. Tardif, S. Nattel, R. St. Arnaud, S. Dedhar, and W. J. Muller. 2006. Targeted ablation of ILK from the murine heart results in dilated cardiomyopathy and spontaneous heart failure. *Genes Dev.* **20**:2355–2360.
84. Witt, S., A. Zieseniss, U. Fock, B. M. Jockusch, and S. Illenberger. 2004. Comparative biochemical analysis suggests that vinculin and metavinculin cooperate in muscular adhesion sites. *J. Biol. Chem.* **279**:31533–31543.
85. Wu, J. C., R. Y. Tsai, and T. H. Chung. 2003. Role of catenins in the development of gap junctions in rat cardiomyocytes. *J. Cell. Biochem.* **88**:823–835.
86. Xu, W., H. Baribault, and E. D. Adamson. 1998. Vinculin knockout results in heart and brain defects during embryonic development. *Development* **125**:327–337.
87. Yamada, S., S. Pokutta, F. Drees, W. I. Weis, and W. J. Nelson. 2005. Deconstructing the cadherin-catenin-actin complex. *Cell* **123**:889–901.
88. Zemljic-Harpf, A. E., S. Ponrartana, R. T. Avalos, M. C. Jordan, K. P. Roos, N. D. Dalton, V. Q. Phan, E. D. Adamson, and R. S. Ross. 2004. Heterozygous inactivation of the vinculin gene predisposes to stress-induced cardiomyopathy. *Am. J. Pathol.* **165**:1033–1044.
89. Zhou, J., J. Qu, X. P. Yi, K. Graber, L. Huber, X. Wang, A. M. Gerdes, and F. Li. 2007. Upregulation of gamma-catenin compensates for the loss of beta-catenin in adult cardiomyocytes. *Am. J. Physiol. Heart Circ. Physiol.* **292**:H270–H276.
90. Ziegler, W. H., R. C. Liddington, and D. R. Critchley. 2006. The structure and regulation of vinculin. *Trends Cell Biol.* **16**:453–460.